Treatment with a CD40 Antagonist Antibody Reverses Severe Proteinuria and Loss of Saliva Production and Restores Glomerular Morphology in Murine Systemic Lupus Erythematosus

Stuart J. Perper, Susan V. Westmoreland, Jozsef Karman, Rachel Twomey, Jane Seagal, Rui Wang, Bradford L. McRae, and Stephen H. Clarke

CD40 is a costimulatory receptor on APCs that is critical for the induction and maintenance of humoral and cell-mediated immunity. Accordingly, CD40 and its ligand, CD40L, have long been considered targets for the treatment of autoimmune diseases. We developed a rat/mouse chimeric anti-mouse CD40 antagonist mAb, 201A3, and evaluated its ability to alleviate murine lupus. Treatment of NZB/W-F_1 mice with 201A3 after the onset of severe proteinuria rapidly reversed established severe proteinuria and nephritis and largely restored normal glomerular and tubular morphology. This coincided with a normalization of the expression of genes associated with proteinuria and injury by kidney parenchymal cells. Anti-CD40 treatment also prevented and reversed loss of saliva production and sialadenitis. These effects on kidney and salivary gland function were confirmed using mice of a second strain, MRL/Mp-*lpr*/*lpr*, and extended to alleviating joint inflammation. Immunologically, anti-CD40 treatment disrupted multiple processes that contribute to the pathogenesis of systemic lupus erythematosus (SLE), including autoreactive B cell activation, T effector cell function in target tissues, and type I IFN production. This ability to disrupt disease-critical immunological mechanisms, to reverse glomerular and tubular injury at the cellular and gene expression levels, and to confer exceptional therapeutic efficacy suggests that CD40 is a central disease pathway in murine SLE. Thus, a CD40 antagonist Ab could be an effective therapeutic in the treatment of SLE. ***The Journal of Immunology*****, 2019, 203: 58–75.**

Systemic lupus erythematosus (SLE) is an autoimmune disease triggered by a loss of immunological tolerance, as exemplified by the presence of autoantibodies to numerous nuclear and cytoplasmic Ags (1, 2). Although this disease can affect any organ, the clinical manifestations of the disease vary considerably among patients. This is thought to arise from differences between patients in the operant pathogenic mechanisms (3). Although our understanding of these pathogenic mechanisms in human SLE remains poor, several key processes are known. They include the following: 1) autoreactive B cell activation to generate immune complexes that can initiate inflammation where they deposit, 2) autoreactive T effector cell function (e.g., T_H1 and T_H17) at sites of inflammation, and 3) plasmacytoid dendritic cell (pDC) production of type I IFN (IFN-I) that can directly cause tissue injury and can amplify autoreactive B and T cell activation (4).

AbbVie Bioresearch Center, Worcester, MA 01605

ORCID: 0000-0002-5959-5139 (J.S.).

Received for publication January 11, 2019. Accepted for publication April 29, 2019.

Address correspondence and reprint requests to Dr. Stephen H. Clarke, AbbVie Bioresearch Center, 100 Research Drive, Worcester, MA 01605. E-mail address: stephen.clarke@abbvie.com

The online version of this article contains supplemental material.

Abbreviations used in this article: APCy, allophycocyanin; BUV, Brilliant Ultra-Violet; BV, Brilliant Violet; GC, germinal center; IFN-I, type I IFN; MRL/lpr, MRL/Mp-*lpr*/*lpr*; mu, murine; PAS, periodic acid–Schiff; pDC, plasmacytoid dendritic cell; RO, receptor occupancy; sCD40L, soluble CD40L; SLE, systemic lupus erythematosus; Tfh, T follicular helper.

The CD40/CD40L pathway is fundamental to both humoral and cell-mediated immunity (5), and targeting it could affect multiple pathogenic processes in SLE. CD40 is constitutively expressed by APCs (B cells, dendritic cells, and macrophages) and provides an activating signal and can be induced on many nonhematopoietic cells, including parenchymal cells of the kidney, skin, and salivary gland. CD40L is expressed mainly by activated T cells and platelets but is also shed by platelets and present in blood as a soluble protein (soluble CD40L [sCD40L]) (6, 7). CD40 signaling on APCs contributes to numerous cell functions, most notably germinal center (GC) formation and persistence and effector T cell differentiation and activation (5). Moreover, CD40 signaling may be required for robust IFN-I production by pDCs (7). Thus, the involvement of the CD40/CD40L pathway in multiple SLE pathogenic processes suggests that targeting this pathway could be efficacious in SLE.

We have developed a rat/mouse chimeric anti-mouse CD40 antagonist Ab that exhibits no agonist activity. We show, in this study, that prophylactic administration of this Ab to mice of two SLE-prone strains blocks the development of nephritis, arthritis, and sialadenitis. Moreover, therapeutic anti-CD40 administration after the onset of severe proteinuria reverses proteinuria and increases saliva production. In addition to disrupting multiple immunological processes relevant to SLE pathogenesis, anti-CD40 treatment normalizes parenchymal cell gene expression and reverses glomerular damage. This compelling therapeutic response in murine SLE suggests that CD40 antagonism may be a promising therapeutic strategy for the treatment of SLE.

Materials and Methods

Mice

Female NZB/W-F_1 mice (Jackson Labs Technologies) at 26 wk of age, female MRL/Mp-*lpr*/*lpr* (MRL/lpr), and C57BL/6J mice (Jackson Labs

Technologies) at 10 or 6–8 wk of age, respectively, were used. Mice were housed in an American Association for the Accreditation of Laboratory Animal Care–accredited specific pathogen-free facility under a 12/12 h light/dark cycle with food and water provided ad libitum. All studies involving animals were reviewed and approved by the AbbVie Institutional Animal Care and Use Committee.

201A3, a mouse-specific antagonistic anti-CD40 mAb

201A3 is an anti-mouse CD40 rat/mouse chimera with rat variable domains and mouse IgG2a/κ C region domains, and it exhibits no ability to bind human CD40. It was prepared internally and stored at −80°C in the AbbVie Biologics Pharmacy, Worcester, MA.

Sprague Dawley rats were immunized by hock immunizations using recombinant murine (mu)CD40/human IgG1 fusion protein (R&D Systems). Serum titers were assessed by binding to muCD40-overexpressing HEK 293 cells. Lymph node cells were isolated from immunized animals and fused with myeloma NS0 cells by electrofusion. Primary hybridoma hits were identified by ELISA based screening using recombinant muCD40/human IgG1 (the immunogen), followed by flow cytometry assay using muCD40-overexpressing HEK293 cells. To identify hybridomas producing Abs with potential blocking activity, we developed an ELISA-based blocking assay. The anti-mouse CD40 Ab clone 201A3 was identified, and the V_H/V_L cDNA of the hybridoma clone was amplified by RACE PCR using Ig C region–specific primers. The variable domains were converted and expressed as a rat/mouse chimera with rat Fv and mouse IgG2a/κ constant regions.

Functional characterization of 201A3 in vitro

Primary splenocytes were isolated from C57BL/6J mice by homogenizing spleens between glass slides in Dulbecco PBS without CaCl or MgCl (Life Technologies). RBCs were lysed using RBC Lysis Buffer (eBioscience). Cells were washed and resuspended in RPMI 1640 containing 10% FBS (HyClone), 2 mM GlutaMax, 100 μg/ml penicillin/streptomycin (Life Technologies) and 55 μM 2-ME (Life Technologies). To assess agonist activity, 200,000 cells were added per well in triplicate to a 96-well, U-bottom tissue culture plate. Cells were incubated for 2 d with titrated concentrations of mouse mIgG2a (AbbVie), 201A3, or anti-CD40 mAb FGK45 (Bio X Cell). To assess antagonist activity, the same number of cells were incubated for 2 d with 1 μg/ml sCD40L (Lonza Group) in the presence of titrated levels of mIgG2a (AbbVie), 201A3, or anti-CD40 mAb MR1 (Bio X Cell). Cells from agonist and antagonist assays were harvested, washed, and resuspended in Dulbecco phosphate-buffered saline without CaCl or MgCl (Life Technologies) plus 2% BSA (Sigma-Aldrich) and labeled with LIVE/DEAD Near-IR Dead Cell Stain Kit (Invitrogen) for 5 min at room temperature. Rat anti-mouse CD16/CD32 Fc block (BD Biosciences) was then added, and cells were incubated for an additional 10 min. Cells were then further labeled with APC-conjugated anti-mouse B220 (RA3-6B2; BioLegend) and PE/Cy7-conjugated anti-mouse CD86 (GL1; BioLegend) and incubated for 30 min on ice. Cells were then washed two times and samples were acquired.

Experimental design and treatment protocols

NZB/W-F_1 prophylactic treatment. A cohort of female NZB/W-F_1 mice at 25 wk of age was tested for urine protein levels. Urine was manually expressed and individually tested for protein levels using Albustix Reagent Strips for Urinalysis (Siemens). Urine protein levels were graded visually based on comparison with color chart provided by the manufacturer: Trace 30, 100, 300, and 2000+ mg/dl. Mice exhibiting urine protein ≤100 mg/dl were randomly assigned to treatment groups (n = 20/group) and ear tagged for individual identification. 201A3 was administered at 15 mg/kg once or twice a week i.p. or 1.5 mg/kg twice a week i.p. starting at 26 wk of age. PBS (vehicle control) was administered twice a week i.p., and prednisolone (Sigma-Aldrich) at 10 mg/kg was administered by daily oral gavage as a positive control. At least weekly thereafter, urine protein levels were determined, and mice exhibiting urine protein ≥300 mg/dl for at least two consecutive weeks were considered to be severely proteinuric. Moribund animals were euthanized, tissues were collected, and the dates were recorded. After 9 wk of treatment, representative animals were euthanized and tissues were collected. Spleens, kidneys, and salivary glands were processed for flow cytometry and/or histologic analysis. Blood was collected by retro-orbital puncture under isoflurane anesthesia or by cardiac puncture. Whole blood was processed for plasma (centrifuged at 15,000 × g for 5 min), decanted, and stored frozen for use in an anti-dsDNA Ab ELISA. Kidneys and salivary glands were collected as mice became moribund throughout the study, and kidneys, salivary glands, and blood were collected at the termination of the study on day 91. For blood RNA, blood was collected by cardiac puncture using heparinized syringes, and 0.5 ml was placed into RNAprotect Animal Blood Tubes (Qiagen). Kidney medial cross-sections and a single salivary gland were fixed in 10% neutral-buffered formalin, processed, and paraffin embedded for histological evaluation. The remainder of each kidney and salivary gland was placed into RNAlater (Thermo Fisher Scientific), held at 4°C overnight, and stored frozen at −80°C prior to further processing for gene expression.

NZB/W-F_1 therapeutic treatment. Three separate therapeutic efficacy experiments were conducted, which were performed identically except for the dosages used. The general experimental scheme for all was as follows. Female NZB/W-F_1 mice at 25 wk of age were tested weekly for urine protein levels as previously described. Mice were enrolled systematically across all treatment groups after exhibiting two consecutive urine protein grades 24 h apart of ≥300 mg/dl. Mice were enrolled between the ages of 26 and 38 wk and averaged 32 wk of age. Treatments were initiated 24 h after the second consecutive elevated urine protein determination. Urine protein levels were monitored at least weekly in all treatment groups thereafter. Recovery from severe proteinuria was defined as at least three consecutive weeks of urine protein grade ≤100 mg/dl. Only the animals that were treated for a minimum of 4 wk (unless becoming moribund) were included in the efficacy analysis. In the first experiment, 201A3 was administered at 15, 3, 0.6, and 0.12 mg/kg twice a week i.p. (n = 14 or 15/group), and for the second and third experiments, 201A3 was administered at 15 mg/kg. Unless noted otherwise, the results shown are from first experiment. PBS (vehicle control) was administered twice a week i.p., and prednisolone was administered as previously indicated.

MRL/lpr mice at 10 wk of age were randomly assigned to treatment groups (n = 18/group). 201A3 was administered at 15, 5, and 1.5 mg/kg twice a week i.p. PBS (vehicle control) was administered twice a week i.p., and prednisolone was administered as previously described. Mice were treated for 9 wk and followed for proteinuria as described. At study termination, kidney, salivary gland, and rear hock joints were collected for histological analysis.

Flow cytometry analysis

Spleens were dissociated to single-cell suspensions using cMACS tubes, autoMACS Rinsing Solution, gentleMACS Dissociator and Miltenyi Spleen Dissociation Kit (Miltenyi Biotec). RBCs were removed from cell suspensions using multispecies RBC lysis buffer (eBioscience). Cells were centrifuged and resuspended in FACS buffer (PBS plus 1.5% heat inactivated FBS; Invitrogen plus 0.02% sodium azide; Sigma-Aldrich) containing 1:200 of rat anti-mouse CD16/CD32 Fc block (BD Biosciences) and LIVE/DEAD Fixable Blue or Near-IR Dead Cell Stain Kit (Invitrogen) and incubated 30 min on ice. After centrifugation and washing in PBS, cells were resuspended and further labeled with Ag specific Abs. The following mAbs specific for murine Ags were purchased from BD Biosciences, BioLegend, and eBioscience: allophycocyanin (APCy)-conjugated CD3 (145-2C11), APCy-conjugated NKp46 (29A1.4), APCy-conjugated Gr-1 (RB6-8C5), APCy-conjugated CD11b (M1/70), Alexa 488–conjugated Ly-77 (GL7), PE-conjugated CXCR4 (L276F12), PE/Cy7-conjugated CD95 (Jo2), Brilliant Violet (BV)421-conjugated CD86 (GL-1), BV6510-conjugated IgD (11-26c.2a), Brilliant Ultra-Violet (BUV)395-conjugated IgD (11-26c.2a), FITC-conjugated CD4 (RM4-5), PerCP/Cy5.5-conjugated CD19 (6D5), PE-conjugated PD-1 (29F.1A12), PE/Cy7-conjugated CD62L (MEL-14), Alexa 647–conjugated ICOS (C398.4A), biotin-conjugated CXCR5 (L138D7), BV605-conjugated CD44 (IM7), BUV395-conjugated CD3 (145-2C11), and BUV395-conjugated CD3 (145-2C11). Brilliant stain buffer (BD Biosciences) was used where BV fluorochrome–conjugated mAbs were used, and SAv-BV421 (BioLegend) was used in conjunction with CXCR5/biotin. Samples were acquired on a FACSCalibur (BD Biosciences) flow cytometer and analyzed with FlowJo software (version 8.5; Tree Star). Compensation controls were prepared using OneComp beads (eBioscience). Total cell numbers were determined by adding AccuCount beads (Spherotech).

Blood $B220^+$ CD40 receptor occupancy assay. Heparinized whole blood collected 72 h after the last dosage of PBS or 201A3 was added to FACS buffer containing 1:200 rat anti-mouse B220 PE/Cy7 (BioLegend) and 20 μg/ml 201A3/APC, previously labeled using Lightning-Link APC Conjugation Kit (Innova Biosciences). Lyse/Fix Buffer (BD Biosciences) was added to each sample and washed prior to analysis using FACSCalibur (BD Biosciences) flow cytometer. CD40 receptor occupancy (RO) was calculated by determining the fractional geometric mean fluorescence intensity of CD40 APC staining on B220-positive cells derived from 201A3-treated animals versus that of the average derived from PBS vehicle control–treated animals.

Anti-dsDNA ELISA

Anti-dsDNA levels were determined using an ELISA. ELISA plates (Easy-Wash Costar) were coated with 50 μg/ml poly-D-lysine (Sigma-Aldrich) in carbonate/bicarbonate buffer (Sigma-Aldrich) overnight at 4°C, washed, and coated overnight at 4°C with calf thymus DNA at 5 μg/ml (Sigma-Aldrich) in carbonate/bicarbonate buffer (Sigma-Aldrich). Plates were washed just prior to use. Standard reference plasma (pool of plasma from 8- to 10-mo-old NZBW-F_1 proteinuric mice), and unknown plasma samples were serially diluted 1:5, starting at 1:50 in 3.0% BSA (Sigma-Aldrich) plus 0.02% sodium azide (Sigma-Aldrich) in PBS and added to DNA-coated plates to create six-point titration curves. Samples were incubated for 1–2 h at room temperature and washed, and peroxidase-linked goat anti-mouse IgG H chain– and L chain–specific Ab (Jackson ImmunoResearch Laboratories) were added at a 1:2000 dilution in PBS containing 3.0% BSA. Plates were incubated for 1–2 h at room temperature and then washed. Tetramethylbenzidine Substrate Solution (Invitrogen) was added, and the reaction was allowed to develop at room temperature until the top dilution (1:50) of the reference standard plasma for each plate reached an OD of 2.7–3.0 when read on a Molecular Dynamics SpectraMax 190 Plate Reader at 650 nm. The reaction was stopped with the addition of 1N HCL, and the final absorbance read at 450 nm. A four-parameter logistic model was used for curve fitting of each titration curve using SoftMax Analysis Software v.6.0 and EC_{50} determinations were used for each sample.

Pilocarpine induced saliva collection

At study day 69, all animals on study, plus a group of eight 17-wk-old NZB/W-F_1 mice, were anesthetized using isoflurane anesthesia, and 60 μg pilocarpine nitrate (Sigma-Aldrich) was administered i.p. Two minutes after pilocarpine injection saliva was collected, for 8 min, while under continued anesthesia, preweighed children's safety swabs inserted into the mouth, and difference in weight postcollection was calculated.

Histology analysis of kidney and salivary gland sections

Kidney and salivary gland samples were fixed in 10% neutral buffered formalin and processed in paraffin and embedded in blocks. Blocks were sectioned at 3 μm and mounted on glass slides prior to performing immunohistochemistry. Kidney samples were multiplexed using the Leica Bond autostainer with IBA1 (Wako) and CD3 (Thermo Fisher Scientific) with a methyl green counterstain (Poly Scientific). Vectra spectral imaging system was used to collect at least 20 20×-high-power images of CD3- and IBA1-stained kidney sections. The 20×-high-power, high-resolution images were then subjected to image analysis algorithms in the inForm software (PerkinElmer). Images were analyzed for IBA1 and CD3 area as a measure of overall inflammation in the kidney. Images were collected within the cortex region of the kidney while avoiding lymphoid aggregates. The inForm algorithm set that was used has three algorithms: the first thresholds the staining for IBA1 and CD3 in spectrally imaged files to eliminate background/extraneous stain. The subsequent algorithms segment the tissue into tissues of interest and quantifies either CD3 or IBA1 in the red–green–blue images produced from the first algorithm.

Salivary glands were stained with CD45 (BD Biosciences) and scanned on a Panoramic digital slide scanner (PerkinElmer) at 20×. Analysis of whole-slide images of the salivary glands was performed using Visiopharm software. The analysis involved a two-step process; in the first step, an algorithm identified the whole tissue on the slide, and in the second step, a different algorithm identified the immunolabeled positive pixels in the segmented tissue. The data were processed as the number of positive pixels of the immune cells divided by the total number of pixels associated with the segmented tissue.

Kidneys, a single salivary gland, and both rear paws were collected and fixed in 10% neutral-buffered formalin for a minimum of 24 h. Rear paws were decalcified using Cal-Rite (Richard-Allan Scientific 5501). Kidneys, salivary glands, and decalcified paws were then embedded in paraffin using an automated tissue processor. All samples were sectioned at 5 μm and stained with H&E. Stained slides were evaluated and scored by a veterinary pathologist. Kidneys were separately evaluated for glomerular disease, tubular dilation, and perivascular infiltrates according to the following schemes. Glomerular disease was scaled by the following: 0, no inflammation; 1, segmental thickening of the mesangium (not all glomeruli); 2, segmental to diffuse thickening of the mesangium (most glomeruli); 3, diffuse thickening of the mesangium (up to three times normal thickness), hypercellular glomerulus, increased size of podocytes (cytoplasm and nucleus), and generally no adherences; and 4, diffuse thickening of the mesangium with areas worse than others, may be coagulated proteins or fibrous hypocellular glomerulus, increased size of podocytes (cytoplasm and nucleus), and Bowman capsule epithelium, adherences, and crescents. Tubular dilation was scaled by the following: 0, no inflammation; 1, minimal/mild dilation of a few tubules, either as a focus or multifocally, generally limited to inner stripe of the outer medulla; 2, minimal/mild dilation of up to 20% of the tubules, either as a focus or multifocally, generally limited to the inner stripe of the outer medulla; 3, mild/moderate dilation of up to 50% of the tubules, expands to some areas of the cortex; and 4, mild/moderate dilation of >50% of the tubules, expands throughout the cortex. Perivascular infiltrates were scaled by the following: 0, up to a few rare lymphocytes; 1, a few lymphocytes forming loose aggregates; 2, lymphocytes forming discrete small aggregates; 3, polarized aggregate of lymphocytes that bulge into the lumen of the adjacent vein but fail to fully surround the arcuate artery; 4, lymphocyte aggregate fully, surrounding the arcuate artery and not showing obvious polarization; and 5, lymphocytic infiltrates extending from the adventitia of the arcuate artery into the adjacent connective tissue.

Salivary gland was scaled by the following: 0, no inflammation; 1, rare perivascular infiltrates; 2, one to two small aggregates of perivascular or periductular inflammatory infiltrates; 3, multiple medium-sized aggregates of periductular infiltrates that extend into acinar tissue; 4, multiple large to coalescing periductular aggregates that extend into, compress, or replace acinar tissue.

Paw joints was scaled by the following: 0, no inflammation; 1, rare infiltrates within synovium; 2, frequent infiltrates within synovium and adjacent joint tissue; 3, numerous infiltrates within synovium and adjacent joint tissue; 4, marked infiltrates that expand and replace synovium and adjacent joint tissue. Sum of both rear paw scores were averaged for each group.

Blood, kidney, and salivary gland analysis for gene expression

Homogenization of kidney and salivary gland samples for gene expression. Tissues were removed from RNAlater and placed in 2-ml Eppendorf Tubes (Qiagen) containing one 5-mm diameter stainless steel bead (Qiagen) and then 700 μl of Qiazol (Qiagen) was added to each sample. Samples were placed in a 2 × 24 TissueLyser Adapter Set (Qiagen) of the TissueLyser II (Qiagen). The TissueLyser II was operated for 2 min at 20 Hz, after which, the samples were placed on ice for 1 min. The TissueLyser II was then operated in 2-min increments until samples were fully homogenized. Tubes were briefly centrifuged to bring all liquid to the bottom, and an additional 700 μl of Qiazol was added. Homogenate was frozen at −80°C prior to further processing.

RNA extraction of kidney and salivary gland samples for gene expression. The kidney homogenate was thawed and incubated at room temperature for 5 min and then briefly vortexed and centrifuged. One hundred and forty microliters of chloroform (Sigma-Aldrich) was added to each sample and mixed with vigorous shaking for 15 s. After 3 min of incubation at room temperature, samples were centrifuged at 16,100 × *g* for 15 min at 4°C. RNA was extracted from the clear upper phase with use of Qiagen QIAcube robot using a custom protocol that follows the miRNeasy Mini Handbook (Qiagen) with the addition of an On-Column DNase Digestion with the RNase-Free DNase Set (Qiagen). Samples were eluted in 50 μl of RNase-free water.

RNA extraction of blood samples for gene expression. Samples were thawed and incubated in RNAprotect Animal Blood Tubes overnight at room temperature for complete lysis of the blood cells. Tubes were mixed by inversion and then centrifuged at 5000 × *g* for 3 min at room temperature to pellet the sample, including nucleic acid and protein. Pellet was washed and centrifuged twice with RNase-free water using clean Eppendorf Tubes (Qiagen). Supernatant was removed, and RNA was extracted using Qiagen QIAcube robot with a protocol that follows the RNeasy Protect Animal Blood Handbook (Qiagen). Samples were eluted in 30 μl of RNA elution buffer.

RNA quantification. Qiagen QIAxpert was used to quantify the extracted RNA with the A260 RNA analysis app. Water blank was used for the kidney samples, and an Elution rehydration buffer blank was used for blood samples.

For gene expression by microarray, biotinylated cDNA were prepared according to the Affymetrix WT 2.0 PLUS Reagent Kit from 200 ng total RNA. Following fragmentation and labeling, 3.5 μg of cDNA were hybridized onto the Mouse Gene 2.0 Arrays and placed in GeneChip Hybridization Oven 640 for 18 h at 45°C. Microarrays were washed and stained in the Affymetrix Fluidics Station 450. GeneChips were scanned using the Affymetrix GeneChip Scanner 3000 7G. The data were analyzed with the Affymetrix GeneChip Command Console. Microarray expression data were processed using Command Console (Affymetrix) and the raw (.CEL) files generated were analyzed using Expression Console Software with Affymetrix default Robust Multichip Analysis Gene analysis settings

(Affymetrix). Probe summarization Robust Multichip Analysis, quality control analysis, and probe annotation were performed according to recommended guidelines (Expression Console Software; Affymetrix). The final data analysis was performed using the web-based gene expression data browser. The IFN signature score was calculated as the median expression level of four known IFN-I regulated genes (Ifi27, Ifi44, Ifi44l, and Rsad2). The chemokine gene signature score was calculated the same way using 31 genes found to be expressed in kidney or salivary gland (Supplemental Table I). Median gene expression was analyzed using one-way ANOVA and Tukey pairwise comparisons.

Results

Anti-CD40 Ab 201A3 has antagonist activity

The anti-mouse CD40 mAb 201A3 is a rat/mouse chimera with rat Fv regions and mouse γ2a and κ constant regions and does not cross-react with human CD40. The Fc region lacks FcγR and complement binding abilities because of D265A and N297A mutations (8–10). 201A3 has no agonist activity, as it is unable to induce CD86 expression on mouse primary B cells (Fig. 1A), but it exhibits potent antagonist activity, as it blocks CD40L-mediated upregulation of CD86 on mouse B cells (Fig. 1B). 201A3 will be referred to hereafter as anti-CD40.

Prophylactic treatment with anti-CD40 prevented the development of proteinuria and extended survival in female NZB/W-F_1 mice

To assess the effectiveness of CD40 pathway blockade at abrogating murine SLE, we first determined whether prophylactic treatment would be effective in preventing development of proteinuria and nephritis in NZB/W-F_1 mice. We found that when treatment was begun, before onset of proteinuria at 26 wk of age, anti-CD40 at either 15 or 1.5 mg/kg i.p. twice per week or 15 mg/kg i.p. once per week prevented the onset of proteinuria (Fig. 2A). Consistent with this, anti-CD40–treated mice had significantly fewer splenic GC B cells and T follicular helper (Tfh) cells as determined by flow cytometry indicating that CD40 function (5) was inhibited at the doses administered (Fig. 2B, 2C).

Therapeutic treatment of NZB/W-F_1 mice reversed ongoing proteinuria and nephritis

A more stringent and relevant test of efficacy is to treat therapeutically after the onset of severe proteinuria. Treatment of NZB/W-F_1 mice with PBS, anti-CD40, or prednisolone was begun after the development of severe proteinuria, which we defined as two consecutive, high urine protein measurements (≥300 mg/dl urine protein) 24 h apart, and the mice were monitored weekly for changes in urine protein levels.

Anti-CD40–treated mice exhibited a dosage-dependent reduction in splenic GC B cells and Tfh cells in comparison with PBS control mice (Fig. 3A), indicating effective blockade of CD40 function at only the two highest dosages. Whereas PBS-treated mice remained proteinuric for the duration of the study and became moribund, the average urine protein levels were significantly reduced, and mean survival significantly extended in mice of the 15 and 3 mg/kg anti-CD40 dosage groups (Fig. 3B, 3C). Mice in the 0.6 and 0.12 mg/kg anti-CD40 cohorts were not significantly different from those of the PBS control cohort in average urine protein levels and mean survival. Although daily prednisolone treatment significantly reduced GC B and Tfh cell numbers, the average urine protein level and mean survival were not significantly different from PBS controls (Fig. 3A–C).

The percentage of mice that recovered following anti-CD40 treatment was also dosage dependent. Recovery from severe proteinuria was defined as three or more consecutive weeks of urine protein ≤ 100 mg/dl. Eighty-seven and fifty-three percent of mice

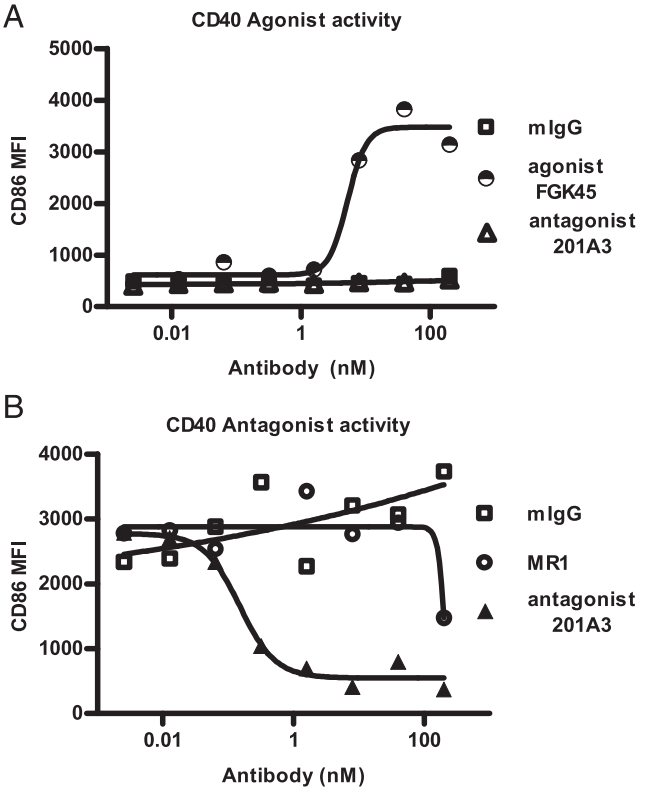

FIGURE 1. Mouse-specific anti-CD40 mAb 201A3 exhibited antagonist activity, but not agonist activity. (**A**) 201A3 was unable to induce CD86 expression on mouse primary B cells after 2 d of culture, as measured by flow cytometry, in contrast to a known agonist Ab, FGK45. (**B**) 201A3 blocked mouse B cell upregulation of CD86 in response to CD40L (1 μg/ml). MR1, the control hamster anti-mouse CD40L Ab, blocked CD86 upregulation but required >100 nM.

in the 15 and 3 mg/kg groups, respectively, recovered from severe proteinuria (both significantly different from PBS control group), whereas only 7% of mice recovered from severe proteinuria in the 0.6 mg/kg group, and none of the mice recovered in the 0.12 mg/kg group (Table I). The average time to recovery was just 13 d for anti-CD40–treated mice. Prednisolone treatment had a modest, but NS, effect on recovery from severe proteinuria (21%). No mice in the PBS control group recovered from severe proteinuria.

Previous studies have demonstrated that nearly full CD40 RO with anti-CD40 is required to inhibit CD40L-mediated signaling in vitro (data not shown). In this study, recovery from proteinuria correlated with CD40 RO on peripheral blood B cells. At the two efficacious doses, there was nearly complete RO, whereas at the two low doses, RO was very low or undetectable (Supplemental Fig. 1).

Efficacy required continuous exposure to anti-CD40

To determine the durability of anti-CD40 treatment, dosing was discontinued for a representative subset of mice from Fig. 2 that had been prophylactically treated, and the mice followed for the development of proteinuria. Mice from all groups developed proteinuria, but the timing of its onset was dosage dependent. Mice in the low-dosage cohort (1.5 mg/kg) were the first to relapse, followed by the 15 mg/kg once per week cohort, and then the 15 mg/kg twice per week cohort (Fig. 4A). Survival followed the same pattern (Fig. 4B). This timing of onset corresponded to loss of exposure (data not shown) and RO (Fig. 4C). Thus, we conclude that efficacy with the Ab 201A3 requires continuous inhibition of CD40 function and does not induce long-term protective mechanisms in these mice.

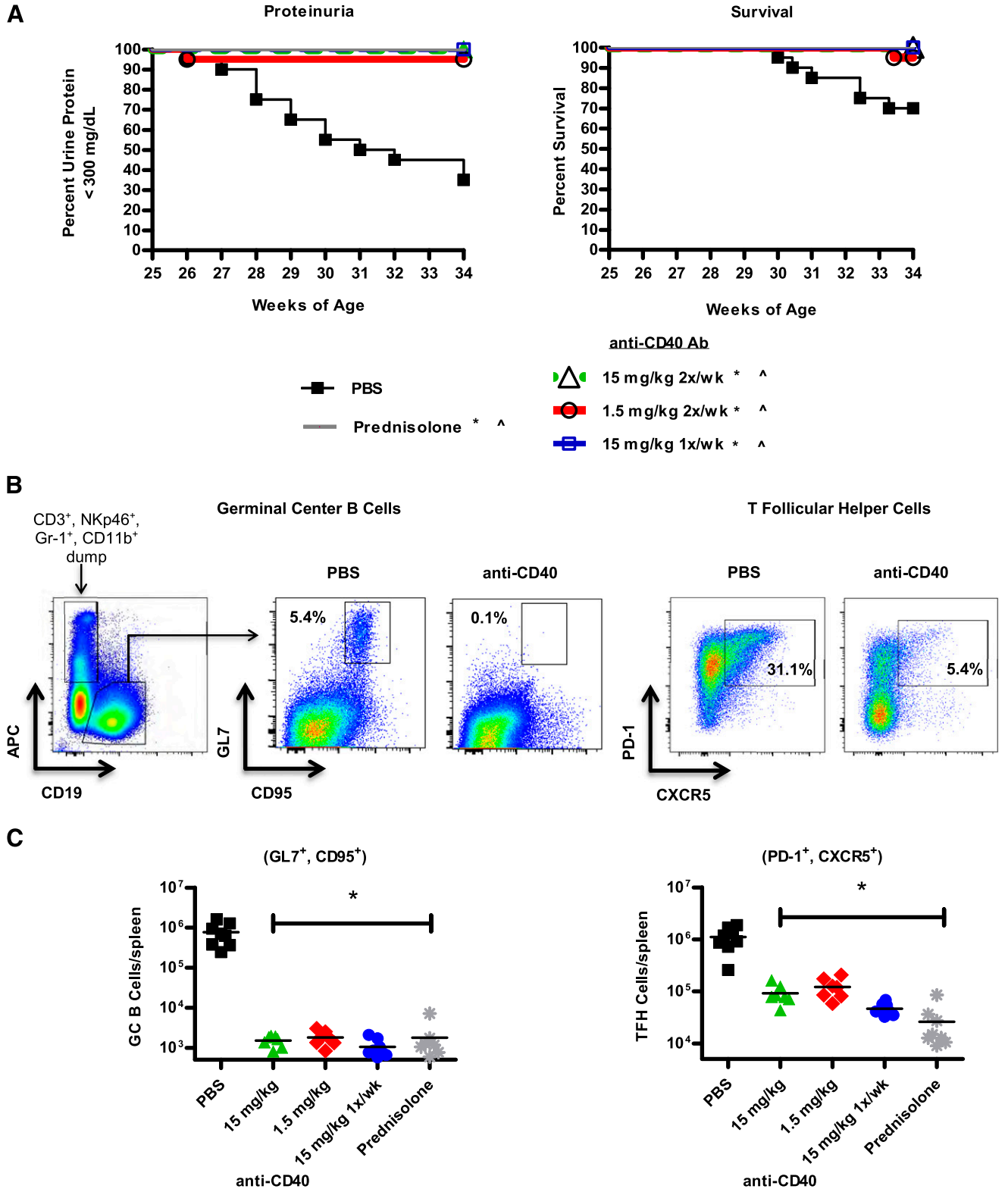

FIGURE 2. Prophylactic treatment of NZB/W-F_1 mice with anti-CD40 mAb 201A3 blocks proteinuria development while extending survival. Non-proteinuric female NZB/W-F_1 mice were enrolled in the study at 26 wk of age and treated as indicated for 9 wk. (**A**) Kaplan–Meier curves show the percentage of NZB/W-F_1 mice that remain nonproteinuric, defined as < 300 mg/dl, and survival of prophylactically treated mice over the 9 wk course of the experiment ($n = 20$ per group). $p < 0.05$, Mantel–Cox survival analysis in comparison with PBS control mice. *, urine protein; ^, survival. (**B**) Representative histograms are shown of the gating scheme for splenic GC B cells and Tfh cells from 35-wk-old female NZB/W-F_1 mice that had been treated prophylactically for 9 wk with PBS or 201A3. GC B cells were identified by negative selection of $CD3^+$, $NKp46^+$, $Gr\text{-}1^+$, and $CD11b^+$, followed by positive gating for $CD19^+$ and finally coexpression of $CD95^+$ and $GL\text{-}7^+$. Tfh cells were gated as $CD4^+$, $CD44^{high}$, $CD62^{low}CXCR5^+$, and $PD\text{-}1^+$. (**C**) Graphs show the total number of GC B and Tfh cells per spleen ($n = 7$ or 8). *$p < 0.05$ one-way ANOVA from PBS control animals.

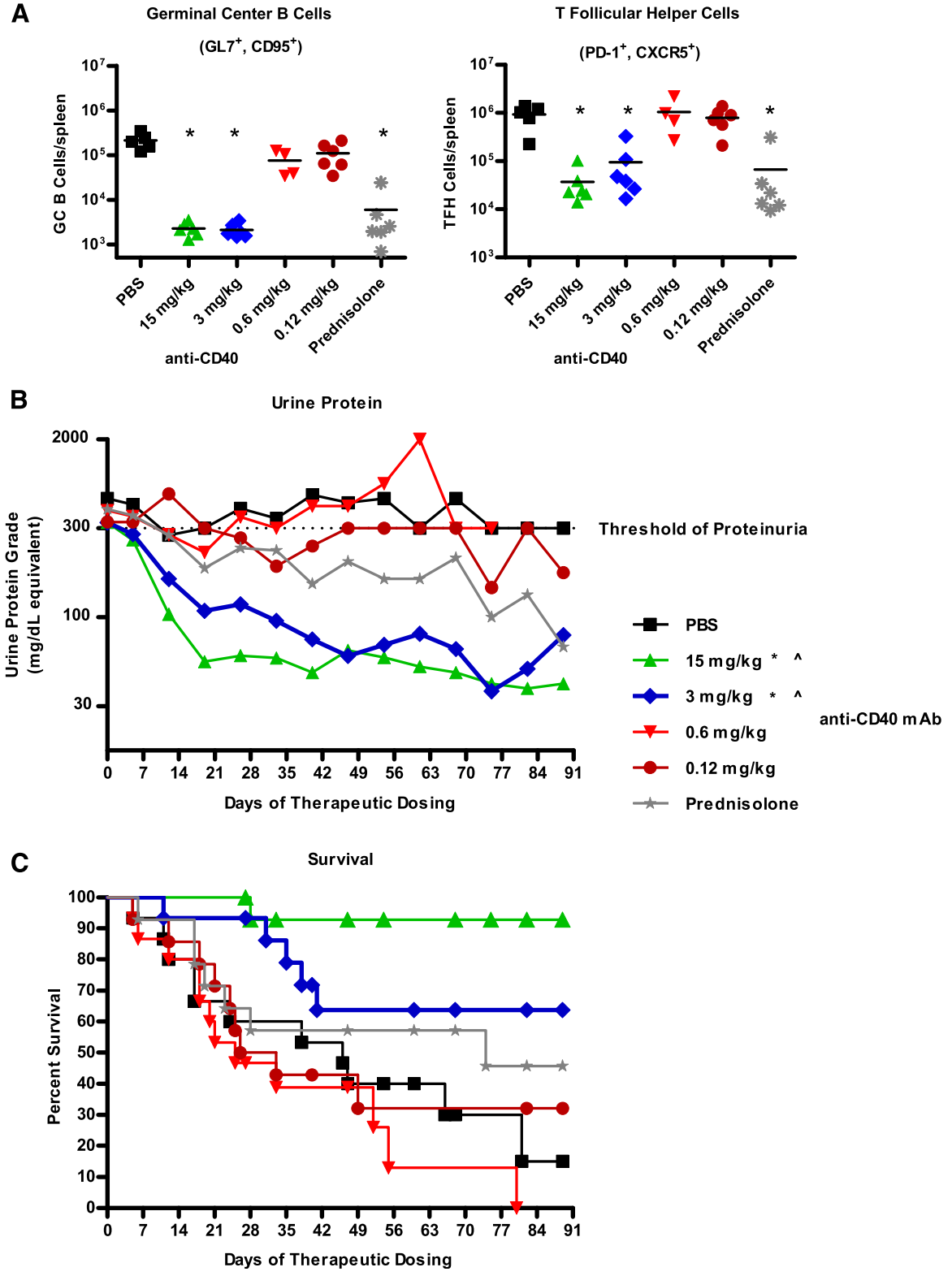

FIGURE 3. Therapeutic treatment of female NZB/W-F_1 mice with anti-CD40 mAb 201A3 reversed severe proteinuria and extends survival. Beginning at 26 wk of age, NZB/W-F_1 mice were monitored for the development of proteinuria and enrolled into a therapeutic study when they reached ≥300 mg/dl of urine protein. (**A**) The numbers of GC B cells and Tfh cells per spleen, determined as described in Fig. 2, are shown ($n = 4$–6). *$p < 0.05$, one-way ANOVA compared with PBS control. (**B**) Shown are the average urine protein levels of treated mice and (**C**) Kaplan–Meier graph showing percent survival following treatment with PBS, 201A3, or prednisolone ($n = 14$ or 15 per group). Note that because this study required a rolling enrollment the *x*-axis is days of dosing rather than age. Treatment duration was from 4 to 12 wk. The dotted line at 300 mg/dl is the threshold of proteinuria that triggered the initiation of treatment. $p < 0.05$ using repeated measures ANOVA and log-rank Mantel–Cox survival test, respectively. *, urine protein; ^, survival.

Table I. Recovery from severe proteinuria and reduction of morbidity by therapeutic treatment with anti-CD40

Group	Total *n*	Recovered *n*	Recovery (%)	Days to Recovery (Mean ± SE)	Morbidity (%)
Vehicle (PBS)	15	0	0	—¶	73
Prednisolone	14	3	21	25 ± 10	50
Anti-CD40					
15 mg/kg	15	13	87*†	13 ± 2	7‡§
3 mg/kg	15	8	53*†	13 ± 3	33
0.6 mg/kg	15	1	7	5 ± 0	80
0.12 mg/kg	14	0	0	—¶	64

*$p < 0.05$ using Fisher exact test compared with vehicle group, †$p < 0.05$ using Fisher exact test compared with prednisolone group, ‡$p < 0.05$ using Mantel–Cox survival analysis compared with vehicle group, §$p < 0.05$ using Mantel–Cox survival analysis compared with prednisolone group, ¶no recovery occurred.

Anti-CD40 treatment reduced kidney inflammation

At the terminus of the therapeutic study, kidneys were evaluated histologically to determine the effect of anti-CD40 treatment on inflammation. We used immunohistochemistry analysis to identify myeloid cells ($IBA1^+$) and T cells ($CD3^+$). Anti-CD40 dosage dependently reduced the number of myeloid cells and T cells in the kidney. This is seen in representative images of the glomeruli (Fig. 5A) and by image analysis quantifying the amount of IBA1 and CD3 staining in whole-kidney sections (Fig. 5B, 5C). IBA1 and CD3 staining in the kidney in mice treated with high-dosage anti-CD40 and prednisolone were not statistically different from young prediseased mice (Fig. 5B, 5C). We performed an analysis at the time treatment was initiated (referred to as baseline) and found that $IBA1^+$ myeloid cells and $CD3^+$ T cells had already infiltrated the kidney, albeit to a lesser extent than at the terminus (Fig. 5B, 5C). Prednisolone treatment eliminated $CD3^+$ and $IBA1^+$ cells from the kidney comparable to high-dosage anti-CD40. B cells are also eliminated based on B220 staining in anti-CD40 (15 mg/kg cohort) treatment and prednisolone treatment (data not shown). Thus, high-dosage anti-CD40 markedly reduced the numbers inflammatory cells of multiple hematopoietic lineages in the kidney to levels like those of young prediseased mice.

Therapeutic treatment with anti-CD40 also reversed the morphological changes that occur over the course of the disease. We separately scored glomerular disease, tubular dilation, and perivascular infiltration. We observed a dosage-dependent decrease in all three of these scores with anti-CD40 treatment, and in each case, the score for mice treated with anti-CD40 at 15 mg/kg was significantly lower than that for the vehicle-treated mice (Fig. 6A–C). Representative images are shown in Fig. 6D. Glomerular damage is shown with periodic acid–Schiff (PAS; an indicator of extracellular matrix deposition by mesangial cells) and podoplanin staining (Fig. 6D, rows 1 and 2), which, together, showed mesangial thickening, matrix deposition, increased glomerular size, crescent formation, and altered podoplanin expression in vehicle-treated kidneys. Podoplanin staining of kidneys from PBS-treated animals and, to a lesser extent, from baseline animals was more intense and occurred mostly around the perimeter of the glomeruli, in contrast to diffuse and less intense staining in young predisease mice. This suggests that the podoplanin production had decreased in the visceral podocytes with disease but had increased in the parietal layer of podocytes. Following high-dosage anti-CD40 treatment, podoplanin staining returned to the more diffuse and less intense staining pattern seen in kidneys of young predisease controls. Tubular dilation and perivascular infiltration were indistinguishable from young predisease mice (Fig. 6B, 6C, respectively). Images of tubules and perivascular infiltration are shown in Fig. 6D, rows 3 and 4, respectively. Analysis of baseline samples indicated that both glomerular disease and perivascular infiltrate scores were elevated at the time of treatment initiation and, therefore, that high-dosage anti-CD40 induced a decrease. Interestingly, prednisolone, although highly effective at reducing tubular dilation and perivascular infiltration, was not very effective at restoration of glomerular morphology. Prednisolone treatment had no effect on glomerular size, mesangial thickening, or proliferation, and it did not restore normal podoplanin production and distribution within the glomerulus (Fig. 6D, rows 1 and 2). These differences between anti-CD40 and prednisolone may explain why only the former reversed proteinuria.

Normal tubular epithelial cells and glomerular cells are reported to be $CD40^+$ and to increase CD40 expression as disease progresses (11–13). Consistent with this, we observed little CD40 staining on tubular and glomerular cells of young prediseased mice (data not shown) and observed that the staining intensity on tubular and glomerular cells was higher in severely proteinuric kidneys of mice at baseline and after PBS treatment. Prednisolone had little effect on CD40 levels on these cells, indicating that CD40 production was relatively unaffected by steroid treatment. We were unable to detect CD40 expression in kidneys from anti-CD40–treated mice because of competition between the therapeutic and staining Abs.

Anti-CD40 reduced IgG anti-dsDNA levels

Autoantibodies to nuclear Ags are a hallmark of SLE, and NZB/W-F_1 mice exhibit elevated levels coincident with disease development (14, 15). Mice treated therapeutically with anti-CD40 at 15 and 3 mg/kg had significantly lower levels of circulating IgG anti-dsDNA autoantibodies in comparison with those of PBS-treated mice (Supplemental Fig. 2). There was a trend toward decreased IgM anti-dsDNA, IgG anti-RNP Abs, and total IgG and IgM levels, but none were significantly different from PBS control mice (data not shown). These results are consistent with the critical role of CD40 in T-dependent Ab responses.

Therapeutic anti-CD40 treatment restored saliva production and reduced salivary gland inflammation

In parallel to the development of nephritis and proteinuria, NZB/W-F_1 mice develop salivary gland inflammation and salivary gland hypofunction, similar to some SLE patients (16). To determine the effect of anti-CD40 treatment on the salivary gland, we measured saliva production and performed histological analysis of salivary glands. Saliva production was measured in mice after treatment with pilocarpine, a muscarinic receptor agonist that is used clinically for the treatment of xerostomia and experimentally in rodents for the evaluation of saliva output (17, 18). PBS-treated mice produced significantly less saliva than young prediseased mice (Fig. 7A). However, we observed a dosage-dependent

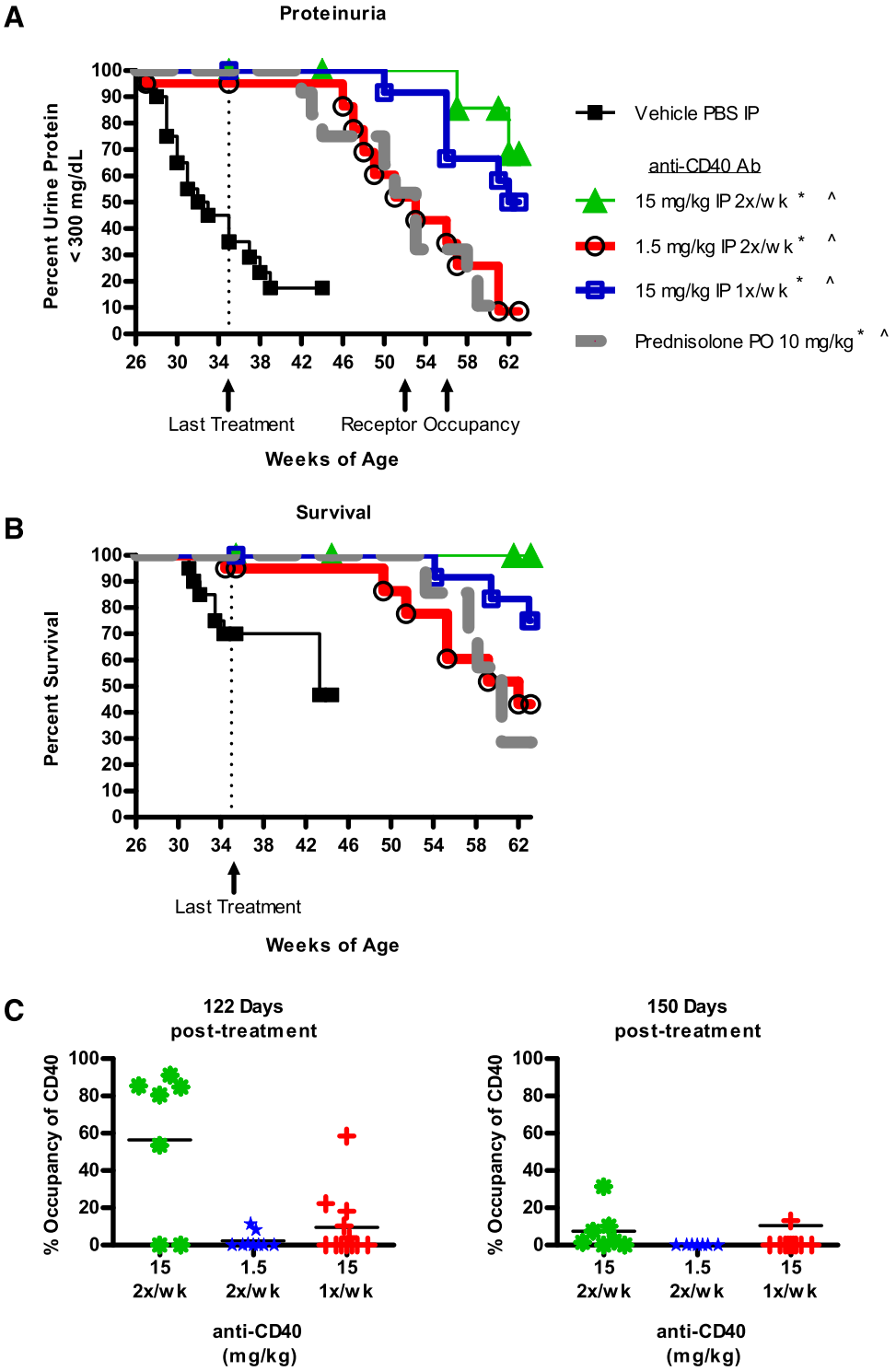

FIGURE 4. Disease relapse occurred in a dosage-dependent fashion following cessation of treatment. NZB/W-F_1 mice used in the prophylactic study shown in Fig. 2 were used to determine whether disease relapse would occur following treatment cessation. (**A** and **B**) Kaplan–Meier graphs showing proteinuria onset (defined as >300 mg/dl of urine protein) and survival are presented. Dotted vertical lines indicate the point (35 wk of age) when treatment was terminated. Number of mice per group: $n = 20$ per group <35 wk of age, $n = 11$–12 per group >35 wk. of age. $p < 0.05$ Mantel–Cox survival analysis. *, proteinuria; ^, survival. (**C**) Calculated blood CD40 RO on $B220^+$ B cells at two time points posttreatment (122 and 150 d). Number of animals per group: 15 mg/kg twice per week ($n = 7$ at 122 d, $n = 7$ at 150 d) 1.5 mg/kg twice per week ($n = 9$ on day 122, $n = 7$ on day 150), 15 mg/kg once per week ($n = 12$ on day 122, $n = 11$ on day 150).

improvement over PBS-treated mice in saliva output with anti-CD40 treatment; mice treated at 15 and 3 mg/kg anti-CD40 exhibited saliva production levels like those of prediseased control mice. Prednisolone had no effect on saliva production. In a separate experiment, we demonstrated that mice treated at 15 mg/kg anti-CD40 had improved saliva production over baseline (Fig. 7B), indicating that anti-CD40 treatment can reverse the loss of saliva production in this model.

Anti-CD40 therapeutic treatment also affected inflammation of the salivary gland. The percentage of $B220^+$ B cells in the salivary

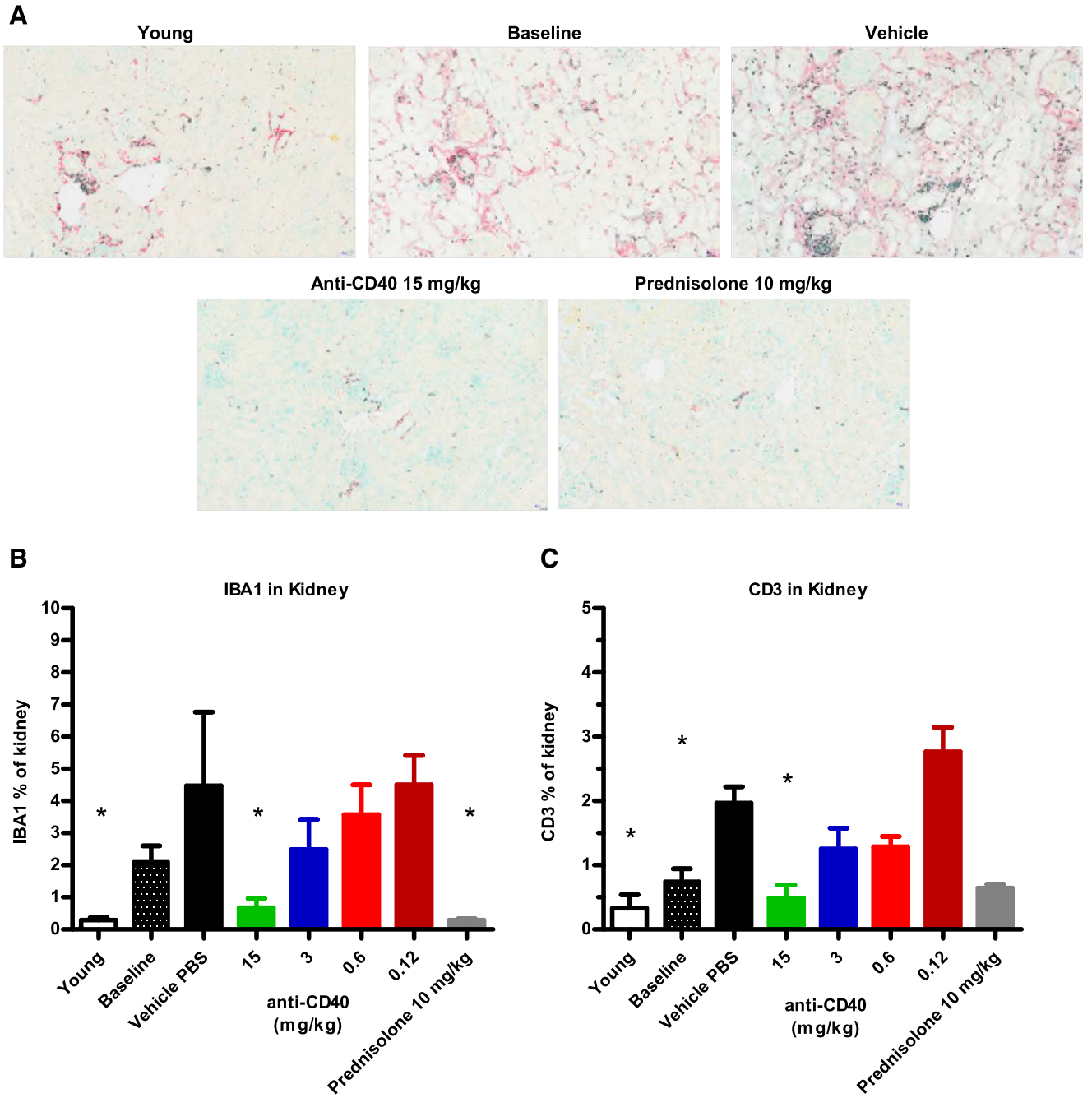

FIGURE 5. Therapeutic treatment with anti-CD40 mAb 201A3 dosage dependently reduced kidney inflammation. (**A**) Representative immunohistochemistry images (original magnification ×20) of kidney sections stained for IBA1 (red) and CD3 (black) are shown. As a measure of overall inflammation, high-power images (original magnification ×20) of CD3 and IBA1 staining of whole-kidney sections were subject to image analysis algorithms in the inForm software (PerkinElmer) to determine the percentage of kidney that stained for IBA1 (**B**) and CD3 (**C**). Numbers of mice per group: young ($n = 5$), baseline ($n = 11$); vehicle/PBS $n = 16$; prednisolone $n = 3$; and anti-CD40 at 15, 3, 0.6, and 0.12 mg/kg ($n = 7$, 10, 5, and 5, respectively). For (B) and (C), the 15 mg/kg anti-CD40 and prednisolone groups are not different statistically from the young prediseased group. $^*p < 0.05$, one-way ANOVA compared with PBS vehicle control mean values ± SD.

gland were determined by image analysis for comparisons across groups. Anti-CD40 treatment had a dosage-dependent effect on the number of B cells in the salivary gland (Fig. 7C), with the mice treated at the high dosage being indistinguishable from young prediseased mice. Like the kidney, prednisolone was as effective as high-dosage anti-CD40. Representative salivary gland immunohistochemistry images are shown in Fig. 7D. These data also indicate that B cell infiltration had reached its peak at baseline, and thus, the decrease after treatment was due to a loss of B cells from the salivary gland.

Anti-CD40 treatment normalized the inflammatory pathways upregulated in diseased kidney and salivary glands

We used transcriptome-wide profiling to evaluate changes in gene expression in kidney and salivary gland that were associated with disease and with therapeutic anti-CD40 treatment. Differentially expressed genes between vehicle and young prediseased mice were evaluated for alterations in their activated pathways using Ingenuity Pathway Analysis software. Pathways were considered significantly upregulated or downregulated if they had a p value of ≤ 0.05 and an absolute z score of ≥ 2. We used p value and z score

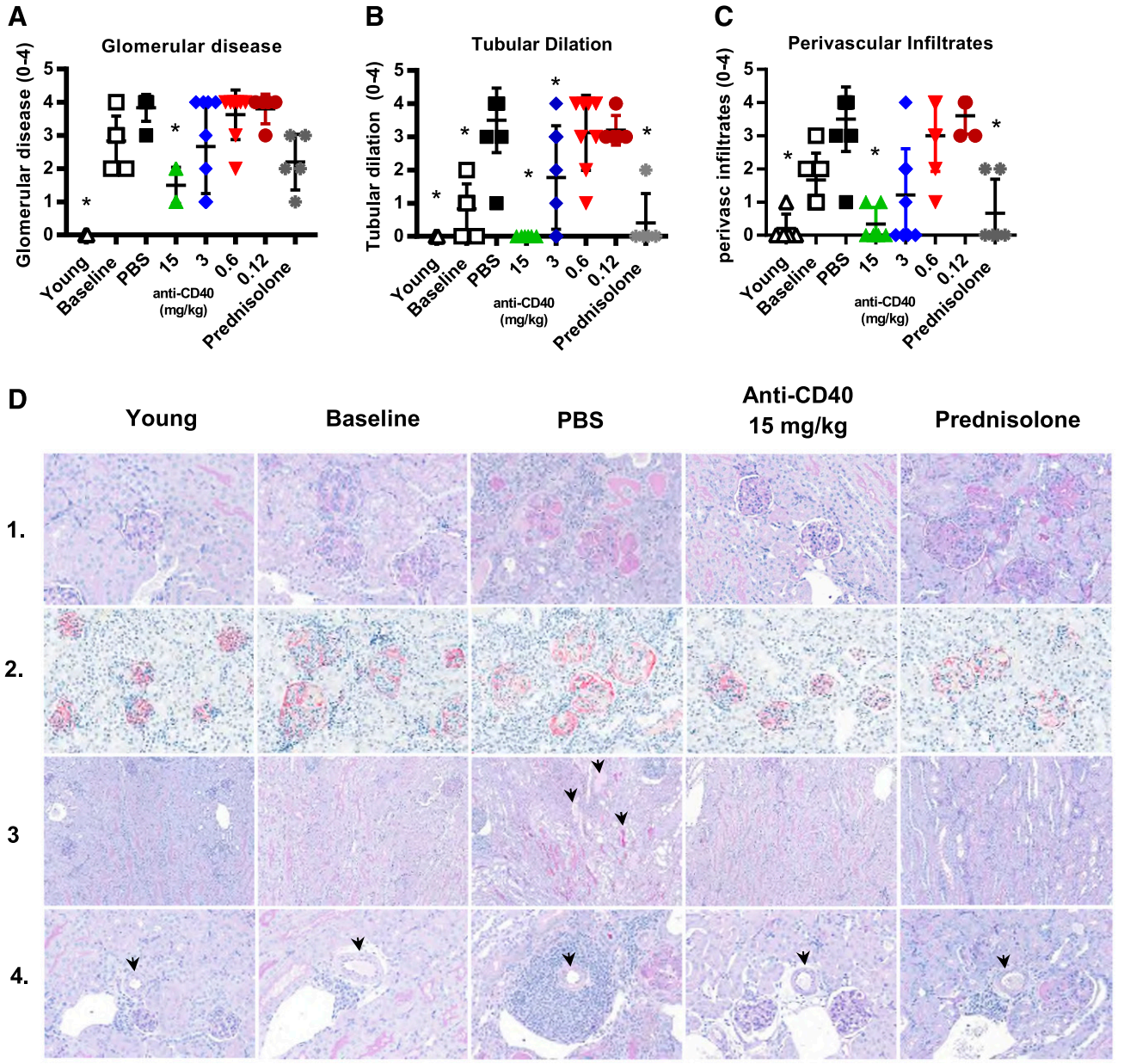

FIGURE 6. Therapeutic treatment with anti-CD40 mAb 201A3 reduced kidney glomerular disease, tubular dilation, and perivascular disease. (**A**–**C**) Kidney histological analysis of glomerular disease, tubular dilation, and perivascular infiltrates for animals treated for a minimum of 4 wk. Scoring system is described for each in the *Materials and Methods*. *$p < 0.05$ Kruskal–Wallis test versus PBS controls. For (C), the 15 mg/kg anti-CD40 and prednisolone groups are not different statistically from the young prediseased group. Numbers of mice per group: young ($n = 5$); baseline ($n = 6$); PBS ($n = 6$); prednisolone ($n = 5$); and anti-CD40 at 15, 3, 0.6, and 0.12 mg/kg ($n = 6$, 9, 8, and 5, respectively) mean values ± SD. (**D**) Representative images of the kidney of mice from the indicated cohorts. All images are at original magnification ×40. Row 1, PAS staining to assess extracellular matrix deposition in and around the glomeruli; row 2, Podoplanin staining to reveal the glomeruli; row 3, PAS stain to reveal the tubules (indicated by arrowheads). Many tubules are open space and appear white, whereas others are filled with protein and stain pink; row 4, PAS staining of sections for IBA1 (red) and CD3 (black) showing inflammation around arcuate arteries (identified by arrowheads).

metrics to assess changes in the activity of Ingenuity-defined canonical pathways. The *p* value is derived from a hypergeometric test to assess the overlap between genes with altered expression and a given canonical pathway. The z score is a measure of the concordance between the expected change in gene expression (based on Ingenuity's curated database) when a given pathway is activated or inhibited and the actual measured change. By these criteria, 47 pathways in the kidney and 38 pathways in the salivary gland showed strong evidence for activation in a comparison between young prediseased and vehicle-treated diseased mice. All but one pathway were associated with inflammation (Supplemental Fig. 3A, 3B). In addition, five pathways were downregulated in the kidney, all of which were metabolic pathways. No downregulated pathways in the salivary gland met the selection criteria. These findings in the kidney are like those reported previously (19). We detected a large overlap in the inflammatory pathways upregulated in kidney and salivary gland (Supplemental Fig. 3C); three-quarters of the pathways upregulated in the salivary gland were also upregulated in the kidney. These included the most significantly upregulated pathways in both tissues and include pathways associated with adaptive and innate immune responses.

Anti-CD40 treatment strongly inhibited the inflammatory pathways that had been upregulated in disease in both kidney and salivary gland (Supplemental Fig. 3A, 3B). In the kidney, the

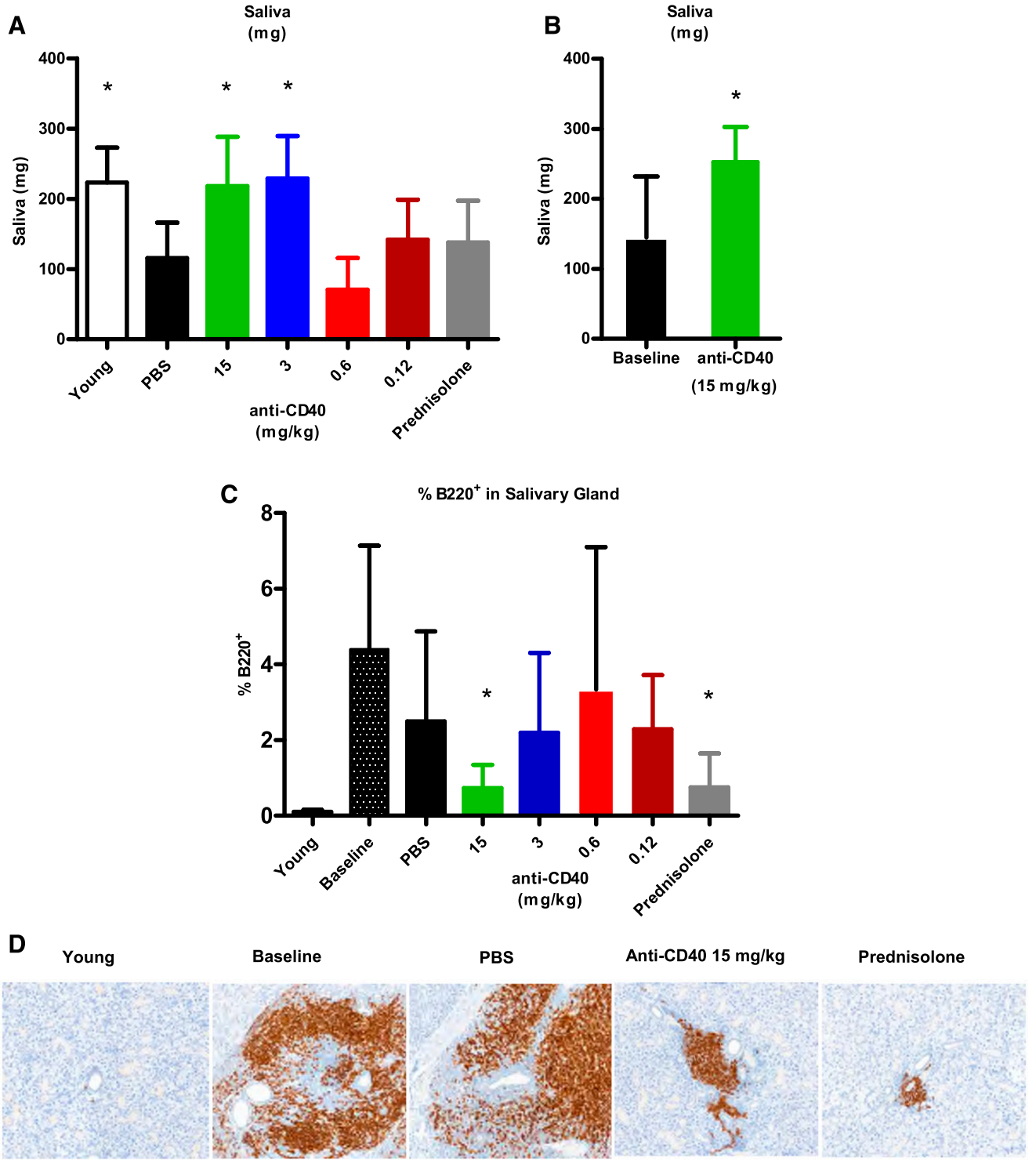

FIGURE 7. Therapeutic anti-CD40 treatment restored saliva production and reduced salivary gland inflammation. (**A**) Saliva production was measured after pilocarpine challenge. Young (n = 8); vehicle/PBS (n = 8); prednisolone (n = 10); and anti-CD40 at 15, 3, 0.6, and 0.12 mg/kg (n = 13, 12, 6, and 7, respectively). (**B**) In a separate experiment, saliva production by anti-CD40–treated mice (15 mg/kg) (n = 7) was compared with untreated mice (n = 6) at baseline. (**C**) Image analysis was used to determine the percentage of salivary glands that stained for B220 at study termination (minimum 4-wk anti-CD40 therapeutic treatment). Numbers of mice per group: young (n = 5); baseline (n = 11); vehicle (n = 16); prednisolone (n = 9); and anti-CD40 at 15, 3, 0.6, and 0.12 mg/kg (n = 7, 10, 15, and 6, respectively). *$p < 0.05$ one-way ANOVA. (**D**) Representative salivary gland images (original magnification, ×40) are presented showing $B220^+$ staining for the different treatment groups.

downregulation of the metabolic pathways was also reversed. Thus, anti-CD40 treatment had far-reaching effects on the pathways altered in disease in both kidney and salivary gland, and, together, with the histologic analysis, indicate that high-dosage anti-CD40 treatment markedly reduced inflammation in the kidney and salivary gland to levels comparable to young prediseased mice.

In addition to examining the overall changes in gene expression in response to anti-CD40 treatment, we evaluated several immune-related gene signatures relevant to SLE. The first is the IFN-I signature. IFN-I

is produced at high levels in a subset of SLE patients and is an important driver of disease (20). Elevated production of IFN-I in SLE is detectable by the increased expression of IFN-I–regulated genes in peripheral blood cells (21–24). A set of four genes (Ifi27, Ifi44, Ifi44l, and Rsad2) was used to derive an IFN signature score, calculated as the median expression level. These genes were used to distinguish IFN^{low} and IFN^{high} SLE patients in SLE phase IIb clinical trials with anifrolumab and sifalimumab (25, 26). The IFN gene signature scores in blood, kidney, and salivary gland of PBS-treated control mice were significantly elevated relative to young mice (Fig. 8A). In addition, the IFN signature score was significantly elevated at baseline in the salivary gland. The IFN signature score in anti-CD40 (15 mg/kg)–treated mice in the blood and kidney were like those in young mice, indicating that anti-CD40 treatment can prevent the development of an IFN signature, and it reversed the IFN signature from baseline in the salivary gland (Fig. 8A). Thus, anti-CD40 treatment appears to block and decrease the production of IFN-I in these mice.

The second immune-related signature we evaluated is a chemokine gene expression signature. As orchestrators of inflammation, chemokines can be produced by infiltrating inflammatory cells as well as parenchymal cells of the kidney and salivary gland (11–13, 27). We found that 31 chemokine genes are expressed in either the kidney or salivary gland or both (Supplemental Table I). Using these 31 genes to compute a gene signature score for each mouse (median expression level of the 31 genes), we found that the chemokine gene signature was increased relative to young controls in vehicle-treated mice in the kidney and salivary glands and was increased at baseline in these tissues (Fig. 8B). There was no significant change in the blood. However, this score was decreased by anti-CD40 therapy in both the kidneys and salivary glands to levels like young prediseased mice, suggesting that anti-CD40 treatment reduced the production of chemokines in both tissues.

Anti-CD40, but not prednisolone, normalizes gene expression of kidney parenchymal cells that are associated with injury and proteinuria

To assess parenchymal cell gene expression, we examined three sets of genes associated with injury and proteinuria. The genes of the first set are associated with monogenic inheritance of proteinuria, or nephrotic syndrome, in humans (28). Of 29 genes linked to nephrotic syndrome, 19 were altered (13 upregulated and 6 downregulated) in kidneys of PBS-treated mice. Most of these genes have been shown, by single-cell RNA sequencing, to be expressed by only podocytes, reflecting the importance of podocytes to the glomerular filtration barrier (28) (Supplemental Table I). Anti-CD40 treatment restored the normal expression level of these nephrotic genes (Fig. 9A, 9B). The altered expression of these genes in diseased mice was unlikely to be due to infiltrating inflammatory cells because, with the exception of only Cfh, they were not expressed by B cells, T cells, macrophages, NK cells, fibroblasts, or neutrophils of normal kidneys (28) and, collectively, they were expressed at much lower levels in whole blood and salivary gland compared with the kidney from diseased mice (data not shown). The second gene set analyzed consisted of 13 genes that encoded proteins associated with epithelial or endothelial cell injury and tubulointerstitial fibrosis (Supplemental Table I). All are known to be expressed by glomerular or tubular cells, although two (Havcr1 and Cst3) are also expressed by hematopoietic cells. As with the nephrotic gene set, they were expressed weakly in whole blood and salivary glands compared with kidneys of diseased mice (data not shown), arguing that the altered expression in kidneys was unlikely to be due to infiltrating inflammatory cells. In comparison with young prediseased mice, these genes were significantly altered (10 upregulated and

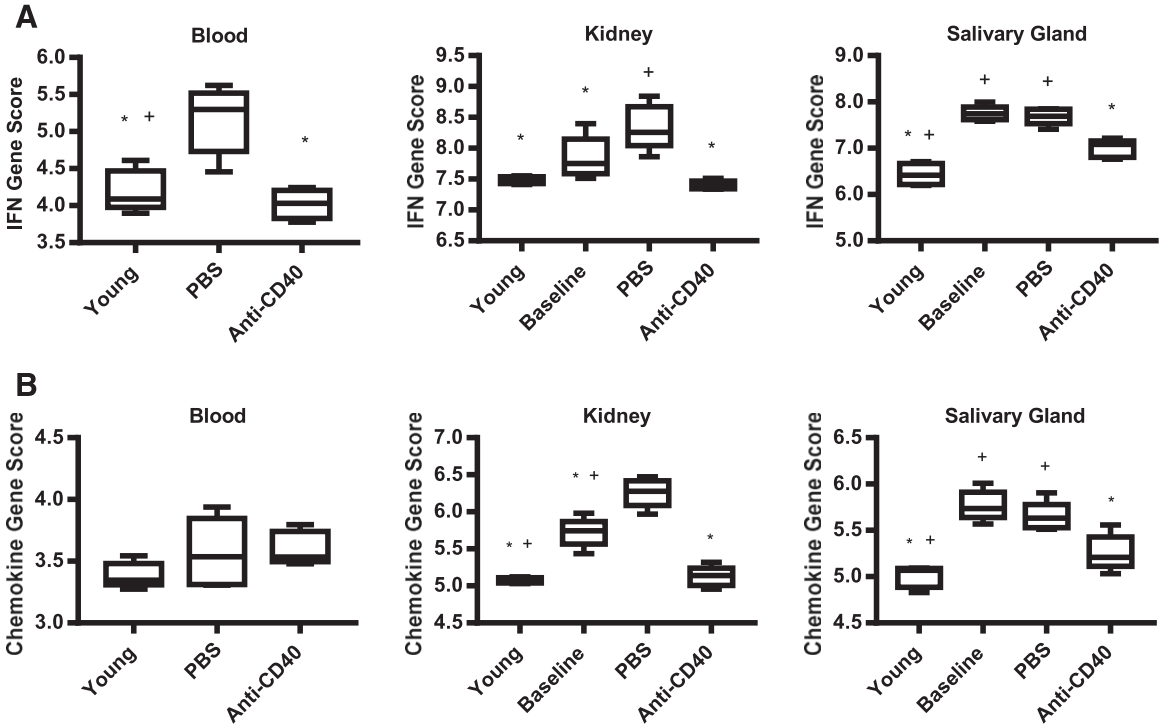

FIGURE 8. IFN and chemokine gene signatures in kidney and salivary gland increased in disease, but are reversed by treatment with anti-CD40. (**A**) The IFN signature score, defined as the median expression level of the 4 IFN responsive genes (Ifi27, Ifi44, Ifi44l, and Rsad2), are graphed for young prediseased mice, PBS-treated mice, untreated baseline mice, and anti-CD40–treated mice (15 mg/kg) (n = 4–6). Blood, kidney, and salivary gland were analyzed and scored separately. (**B**) The chemokine signature score, defined as the median expression level of the 31 chemokine genes that were altered in the kidney or salivary gland in diseased mice listed in Supplemental Table I, are graphed for the same animals shown in (A). $^{*}p < 0.05$ one-way ANOVA verses vehicle PBS, $^{+}p < 0.05$ one-way ANOVA verses anti-CD40.

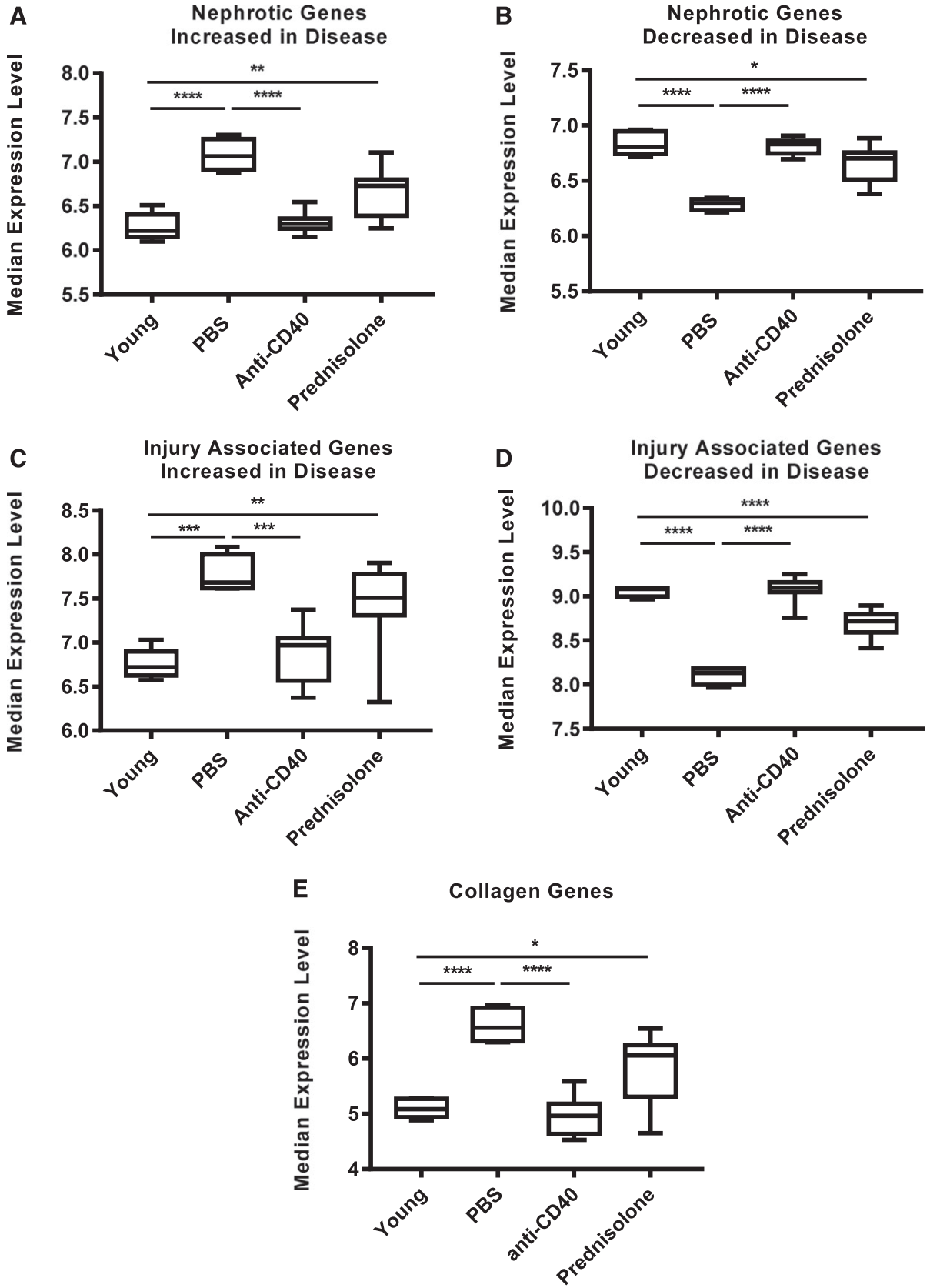

FIGURE 9. Kidney parenchymal cell expression of genes linked to nephrotic syndrome and injury associated genes are altered during disease and normalized by anti-CD40 treatment. The median expression levels of nephrotic syndrome linked genes (**A** and **B**), injury associated genes (**C** and **D**) and collagen genes (**E**) are shown to compare young prediseased mice with the different treatment groups. The genes for each group are listed in Supplemental Table I. Injury associated genes and nephrotic linked genes are divided into two groups: those that are increased during disease and those that are decreased with disease. Young ($n = 5$), vehicle ($n = 4$), and anti-CD40 ($n = 12$) and prednisolone ($n = 9$). *$p < 0.05$, **$p < 0.01$, ***$p < 0.001$, ****$p < 0.0001$ by one-way ANOVA.

3 downregulated) in kidneys from PBS-treated mice (Fig. 9C, 9D), but anti-CD40 treatment normalized the expression levels of both the upregulated and downregulated gene groups. The third set of genes were collagen genes integral to fibrosis (29) (Supplemental Table I). Of the 46 known collagen genes, 18 were upregulated in kidneys of PBS-treated mice, and as with the genes of the previous two sets, anti-CD40 treatment restored their average expression level to be comparable to young prediseased kidneys (Fig. 9E). They, too, were expressed weakly in whole blood and salivary glands compared with kidneys of diseased mice (data not shown). Interestingly, despite the ability of prednisolone to effectively reverse and block inflammation in the kidney, prednisolone only partially restored the expression of the genes of these three groups (Fig. 9A–E). This parallels the inability of prednisolone to restore normal glomerular morphology (Fig. 6) and to reverse proteinuria (Fig. 3, Table I). Altogether, these data suggest that expression of genes associated with proteinuria, injury, and fibrosis in the kidney are upregulated during disease and normalized by high-dosage anti-CD40 treatment.

Anti-CD40 treatment was efficacious in MRL/lpr mice

To confirm the efficacy of anti-CD40 treatment on kidney and salivary gland function and inflammation in a second mouse strain, we evaluated the effect of anti-CD40 on disease in MRL/lpr mice. Disease in MRL/lpr mice develops at 10 to 12 wk of age and involves multiple tissues and organs, including the kidney, joints, skin, and salivary gland. They also develop lymphadenopathy because of a mutation (*lpr*) in the Fas gene that results in rapid morbidity and this precluded the use of a therapeutic dosing strategy and the use of morbidity as an end point. Early morbidity also precluded analysis of skin manifestations, and thus, this analysis focused on kidney, salivary gland, and joints.

PBS, anti-CD40, and prednisolone treatment were initiated at 10 wk of age and continued for 63 d. As shown in Fig. 10A, nearly half of the PBS-treated mice developed severe proteinuria, whereas only 2 of 54 mice treated with anti-CD40 at either 15 or 5 mg/kg developed severe proteinuria. Mice treated with 1.5 mg/kg developed proteinuria comparable to PBS control mice. Prednisolone treated mice were also protected.

Kidney inflammation was assessed at study termination by scoring for glomerular disease and perivascular infiltrates. We observed a dosage-dependent decrease in glomerular disease and perivascular infiltrate scores, with only the 15 mg/kg cohort being statistically significant (Fig. 10B). Although the scores for mice of the 5 mg/kg cohort were quite like those for the 15 mg/kg cohort, they were NS, most likely because of the small number of surviving PBS control animals.

Salivary gland and joint inflammation were also affected by anti-CD40 treatment and showed a dosage-dependent decrease in inflammation scores. At study end, salivary gland inflammation was lower in the 15 mg/kg cohort, although not significantly different from the PBS control cohort, likely because of low numbers of surviving animals (Fig. 10C). Joint inflammation was evaluated for each rear paw, with the score for each mouse computed as the sum of their two rear paws. At study end, inflammation was undetectable in the joints of mice of the 15 mg/kg cohort, although not significantly different from PBS controls (Fig. 10D). Altogether, the histological analysis of tissues from MRL/lpr mice indicates that prophylactic anti-CD40 treatment blocks inflammation in the kidney, salivary gland, and joints.

Discussion

The CD40/CD40L pathway is a central activation pathway for dendritic cells and macrophages and is required for T-dependent Ab responses (5). However, the role of CD40 in the maintenance and progression of tissue-specific and systemic inflammation has been more difficult to establish because of the lack of appropriate CD40-specific tools. We have generated a novel anti-mouse CD40 antagonist that fully blocks signaling induced by CD40L. We report in this study that, when given therapeutically after the onset of severe proteinuria, anti-CD40 treatment induces recovery from proteinuria in NZB/W-F_1 mice and extends their survival. Recovery is rapid with the decrease in urine protein from $\geq$300 to $\leq$100 mg/dl occurring in an average of just 2 wk. Therapeutic anti-CD40 treatment also restores saliva production in the same mice. Accompanying these changes in function was a reduction in inflammation of the kidney and salivary gland, which is seen at the histologic and gene expression levels. These effects were verified in mice of an independently derived strain, MRL/lpr, and extended to the prevention of joint inflammation. Thus, CD40 antagonism resolves inflammation and restores function to tissues targeted in SLE.

Relapse occurred shortly after the loss of CD40 RO. Thus, the reversal of proteinuria appears to require continuous blockade of CD40 binding to CD40L and likely does not involve the induction of a tolerance mechanism that can maintain remission long after the antagonist Ab has been cleared. In apparent contrast, anti-CD40L treatment may induce long-term tolerance. When given with CTLA-4Ig, it induces both regulatory T cell–dependent and –independent mechanisms that can block graft-versus-host disease (30, 31). In the context of SLE, Mohan et al. (32) showed a delay of ~2 mo in the onset of disease upon prophylactic dosing with an anti-CD40L that was well beyond the time required for its clearance. In addition, a study of Sjogren syndrome in NOD mice showed a long-term delay in disease following anti-CD40L treatment (33). Thus, there may be a difference in the ability to induce long-term tolerance between anti-CD40 antagonist and anti-CD40L treatments that warrants further investigation.

Targeting the CD40/CD40L pathway in mice has previously yielded mixed efficacy results. Prophylactic administration of an anti-CD40L Ab, MR1, to NZB/W-F_1 mice had a partial effect on proteinuria and survival (34), whereas therapeutic administration after the onset of severe proteinuria ($\geq$300 mg/dl) of the same Ab to (SWR X NZB) F_1 mice had little effect (35). In contrast, a PEGylated $F(ab')_2$ anti-mouse CD40L Ab given as a single dose yielded results more in line with the efficacy results reported in this study, although comparison with this work is limited by the administration of only a single treatment (36). The difference from the results reported in this study may be due to the relative abilities of anti-CD40 and anti-CD40L to fully neutralize their targets. Neutralization of CD40L may be the more challenging because of the greater abundance of CD40L, as it is present in circulation as a soluble protein and is expressed by platelets (5, 37, 38), and their levels are elevated in mouse and human SLE (7).

The efficacy seen in this study with an anti-CD40 antagonist appears to be better than most therapeutics tested in mice. The topoisomerase inhibitor irinotecan, a chemotherapeutic clinically used for colorectal cancer, has been shown to decrease proteinuria as effectively as that shown in this study with anti-CD40 treatment, although it was less effective on survival (39). In addition, C reactive protein (CRP) has been shown to be effective when dosed after the onset of severe proteinuria inducing histological changes in the glomeruli like those presented in this study (40). Interestingly, CRP appears to convey a long-term effect. Neither therapeutic strategy appears to be in clinical trials. In contrast to these examples, anti-CD20 and BR3-Fc, individually or in combination, were unable to reverse proteinuria using a design like that used in this study (41). Lowering the proteinuria threshold did not

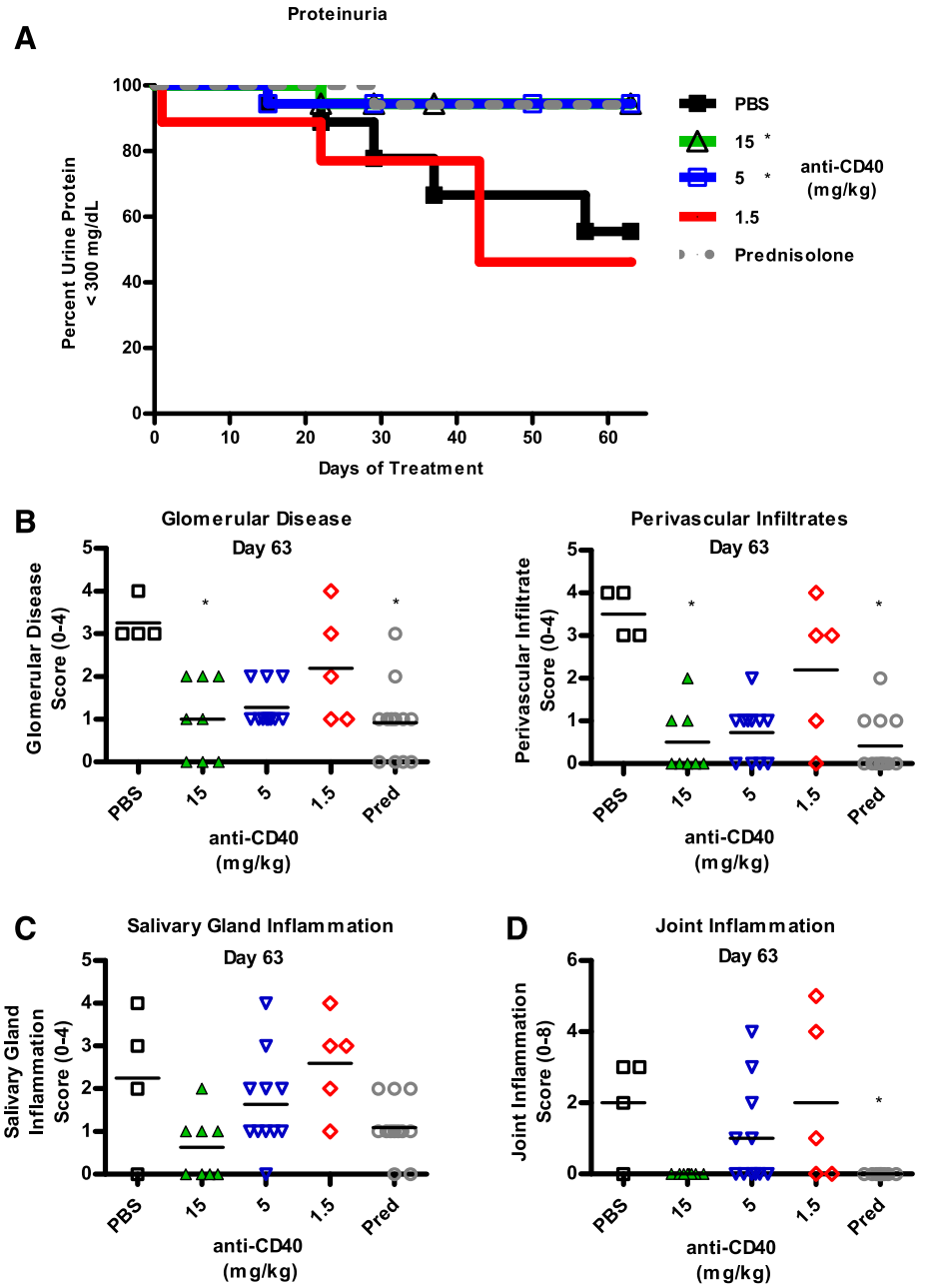

FIGURE 10. Prophylactic treatment of 10-wk-old MRL/lpr mice with anti-CD40 Ab inhibits development of proteinuria, salivary gland inflammation, and joint inflammation. MRL/lpr mice were treated beginning at 10 wk of age with twice-weekly doses of PBS or anti-CD40 at 15 or 1.5 mg/kg, once weekly at 15 mg/kg, or daily with prednisolone. (**A**) A Kaplan–Meier graph of the percentage of mice that are not proteinuric, defined as urine protein ≤300 mg/dl (n = 18 mice per group). *$p < 0.05$ Mantel–Cox survival analysis. Pathological features were determined and scored as described in *Materials and Methods* at study terminus (day 63). (**B**) Glomerular disease and perivascular infiltration scores are graphed. Numbers of mice per group are: PBS (n = 11), prednisolone (n = 12), and anti-CD40 at 15, 5, and 1.5 mg/kg (n = 5, 4, and 11, respectively). (**C**) Salivary gland inflammation scores are graphed. Numbers for mice per group are the same as above. (**D**) Joint inflammation is graphed. Numbers of mice per group are PBS (n = 4), prednisolone (n = 12), and anti-CD40 at 15, 5, and 1.5 mg/kg (n = 8, 11, and 5, respectively). *$p < 0.05$ Kruskal–Wallis test.

improve efficacy (42). We verified in a side-by-side comparison with anti-CD40 treatment that neither therapy alone was able to induce recovery from severe proteinuria (data not shown). CTLA4Ig, a therapeutic that blocks CD28, was also unable to reverse severe proteinuria following therapeutic dosing, except when combined with a second therapeutic, either cyclophosphamide or TACI-Ig (43, 44). Similarly, an anti-IFNAR Ab provided marginal efficacy in two animal models when given therapeutically (45). Thus, anti-CD40 treatment is exceptional in its ability to reverse proteinuria in mice when compared with therapeutics that have been tested in clinical trials, including a surrogate for the Food and Drug Administration–approved therapeutic, belimumab.

Anti-CD40 treatment is highly effective at eliminating inflammatory cells from the kidney and salivary gland. This is evident from the reduction of $CD3^+$ and $IBA1^+$ cells from the kidney after high-dosage anti-CD40 treatment to levels that are not statistically different from those in young prediseased mice and the normalization of inflammatory pathways revealed by gene expression analysis. The mechanism behind the loss of inflammatory cells is unknown, but because this anti-CD40 lacks the ability to bind FcγR and complement, we exclude the involvement of Ab-dependent cellular cytotoxicity and complement depletion. Alternatively, CD40 signaling blockade may affect survival of multiple cell types, as CD40 signaling mediates survival in APCs, which, in turn, could affect T cell survival (46, 47). A nonmutually exclusive and likely possibility is that CD40 blockade causes a loss of inflammatory cells in the kidney and salivary gland by downregulating chemokine production. Chemokines are produced by myeloid cells, and under inflammatory conditions, they can be produced by nonhematopoietic cells, including tubular epithelial cells and mesangial cells of the kidney and epithelial cells of the salivary gland (11–13, 27). CD40 expression is induced on these cells by proinflammatory cytokines (e.g., IFN-γ, IL-1β, and TNF-α), and subsequent engagement by CD40L induces chemokine production. Thus, CD40 antagonism may prevent chemokine production by both myeloid cells and tissue parenchymal cells. In

support, the expression of many chemokine genes in kidney and salivary gland increases substantially with disease, and anti-CD40 reduces their expression to predisease levels. Whether the expression we detect is derived from parenchymal cells, infiltrating inflammatory cells, or both and how much of a role parenchymal cells play in recruiting inflammatory cells to these tissues remains to be determined.

Gene expression by parenchymal cells of the kidney is also altered in disease, as seen by changes in the expression of sets of genes associated with nephrotic syndrome (proteinuria), kidney injury, and fibrosis. Anti-CD40 treatment normalizes the expression of genes from all three of these sets. CD40 is expressed by mesangial cells, podocytes, and tubular epithelial cells under inflammatory conditions, and protein levels on kidney parenchymal cells increases with the development of lupus nephritis (11–13, 27), which we verified in NZB/W-F_1 mice (data not shown). Thus, the ability of anti-CD40 to normalize the expression of these genes raises the possibility that CD40 signaling on parenchymal cells may be responsible for their dysregulation during disease progression. Glomeruli are likely to be continually exposed to CD40L in SLE from circulating sCD40L- and CD40L-expressing platelets (6, 7, 37, 38), even in the absence of local inflammation.

The altered gene expression by parenchymal cells is likely upstream of the abnormal glomerular morphology observed in PBS-treated mice and protein leakage across the glomerular filtration barrier. This barrier is dependent on podocyte function and the integrity of the glomerular basement membrane (48, 49). Many of the genes associated with nephrotic syndrome that we observed to be altered are expressed by podocytes of the glomerulus. Thus, we suggest that blockade of CD40 signaling on glomerular cells to normalize gene expression is critical for reversal of proteinuria. Several lines of evidence support the involvement of CD40 in proteinuria. 1) Platelets can activate mesangial cells by a CD40L-dependent mechanism and can induce podocytes to upregulate matrix metalloproteinase production with potentially deleterious consequences to the glomerular basement membrane, including podocyte attachment (13, 50). 2) In vitro stimulation of human podocytes with an agonist anti-CD40 induces podocyte depolarization and a reduction in size (51), and an anti-CD40 agonist Ab is sufficient to induce mild proteinuria in normal mice and can augment the proteinuria induced by other means (52). 3) CD40 expression by kidney parenchymal cells is required for proteinuria and nephritis in NZB/W-F_1 mice; mice that were engineered to lack CD40 expression by nonhematopoietic cells, but retain expression by hematopoietic cells, fail to develop proteinuria and nephritis (52). Thus, the remarkable ability of anti-CD40 to reverse severe proteinuria may lie in its ability to disrupt CD40 signaling by parenchymal cells of the kidney and suggests that an effective therapy in SLE needs to counter the contributions of parenchymal cells to disease.

This proposed role for CD40 on parenchymal cells provides a possible explanation for why prednisolone is unable to reverse proteinuria. Prednisolone is as effective as high-dosage anti-CD40 at reducing $IBA1^+$ and $CD3^+$ inflammatory cells from the kidney and at normalizing the inflammatory pathways upregulated in the kidney in disease (data not shown). This suggests that, whereas the reduction of inflammatory cells from the kidney may be necessary, it is not sufficient to reverse proteinuria. Significant differences between anti-CD40 and prednisolone treatment include that prednisolone only partially normalizes expression of parenchymal cell genes, including those associated with nephrotic syndrome, and does not restore normal glomerular morphology. Thus, prednisolone may not disrupt critical signaling in kidney parenchymal cells (possibly through CD40) that are needed to reverse glomerular damage and proteinuria. Although prednisolone would diminish glomerular exposure to CD40L on T cells through its ability to markedly reduce inflammatory cells from the kidney, it may not affect exposure of the glomerular cells to circulating cytokines or sCD40L and CD40L on platelets. Thus, the ability to normalize kidney parenchymal gene expression may be an essential attribute for an efficacious therapeutic in lupus nephritis.

In addition to the effect on kidney parenchymal cells, anti-CD40 blockade affects three key immunological processes: B cell activation, T effector cell function, and IFN-I production. The effect on B cells is evident from the loss of GC B cells and Tfh cells induced by anti-CD40, consistent with the requirement for CD40 in GC formation and persistence (53–55) and a decrease in anti-dsDNA levels. The loss of T cells from the kidney and salivary gland, which would include both Th1 and Th17 cells (56–59), suggests that the T cell–mediated pathogenic mechanisms in the kidney and salivary gland are mitigated. Finally, the reduction in the IFN signature in blood, kidney, and salivary glands suggests that IFN production systemically and locally is diminished, consistent with a requirement for CD40 signaling for efficient IFN-I production by pDCs (7).

Long-term CD40 blockade could increase the risk for serious infection. Hyper-IgM patients that lack CD40 or CD40L experience bacterial, viral, and fungal opportunistic infections within the first year after birth and receive gamma globulin infusions and prophylactic antibiotics to compensate for the inability to make IgG and IgA (60). However, unlike hyper-IgM patients, at the time anti-CD40 treatment would be expected to begin, SLE patients will have already developed a long-lived plasma cell population producing Abs of all isotypes, which reflect their antigenic history. Because these cells would not be expected to be adversely affected directly by anti-CD40 treatment, the levels of circulating IgG and IgA should remain high and continue to provide protection from opportunistic infections. This is supported by the observation that, after 11 y of rituximab treatment, IgG, IgM, and IgA levels remain in the normal range for most RA patients (61). Moreover, decreasing Ig levels in these patients is not associated with risk of infection. Susceptibility to viral and fungal infections may be high, because cellular immunity will be affected by CD40 blockade. However, whether the risk is greater than that caused by long-term cyclophosphamide or steroid treatment (62) remains to be determined. Although limited to a short-term treatment of just 10 wk, there were no serious or opportunistic infections in SLE patients with the anti-CD40L therapy dapirolizumab pegol (63).

In summary, we have shown that therapeutic treatment of mice with an antagonist anti-CD40 Ab rapidly reverses ongoing severe proteinuria, reverses loss of saliva production, and reduces inflammation in the kidney, salivary gland, and joints. Mechanistically, anti-CD40 antagonism prevents and disrupts GCs, eliminates T effector cells from the kidney and salivary gland, and reverses the IFN signature in tissues and blood. In addition, our findings implicate CD40 signaling by kidney parenchymal cells in the development of proteinuria because of the ability of anti-CD40 to alter their gene expression, including the expression of genes linked to proteinuria. The ability of anti-CD40 treatment to normalize expression of these genes may be central to its remarkable efficacy, and therefore, we suggest that the ability to normalize organ-specific pathways may be an important criterion in the selection of therapeutics in SLE, in addition to an ability to disrupt disease-critical immune pathways. Altogether, the data presented in this study provide a compelling argument for clinical testing of an anti-CD40 antagonist in SLE.

Acknowledgments

The authors gratefully acknowledge the contributions of Dawna Hartman for assistance with the extensive mouse work and Terri Melim for image analysis of kidney and salivary glands.

Disclosures

All authors are employees of AbbVie. The design, study conduct, and financial support for this research were provided by AbbVie.

References

1. Hochberg, M. C. 1997. Updating the American College of Rheumatology revised criteria for the classification of systemic lupus erythematosus. *Arthritis Rheum.* 40: 1725.
2. Yaniv, G., G. Twig, D. B. Shor, A. Furer, Y. Sherer, O. Mozes, O. Komisar, E. Slonimsky, E. Klang, E. Lotan, et al. 2015. A volcanic explosion of autoantibodies in systemic lupus erythematosus: a diversity of 180 different antibodies found in SLE patients. *Autoimmun. Rev.* 14: 75–79.
3. Ceccarelli, F., C. Perricone, P. Borgiani, C. Ciccacci, S. Rufini, E. Cipriano, C. Alessandri, F. R. Spinelli, A. Sili Scavalli, G. Novelli, et al. 2015. Genetic factors in systemic lupus erythematosus: contribution to disease phenotype. *J. Immunol. Res.* 2015: 745647.
4. Mohan, C., and C. Putterman. 2015. Genetics and pathogenesis of systemic lupus erythematosus and lupus nephritis. *Nat. Rev. Nephrol.* 11: 329–341.
5. Elgueta, R., M. J. Benson, V. C. de Vries, A. Wasiuk, Y. Guo, and R. J. Noelle. 2009. Molecular mechanism and function of CD40/CD40L engagement in the immune system. *Immunol. Rev.* 229: 152–172.
6. Henn, V., S. Steinbach, K. Büchner, P. Presek, and R. A. Kroczek. 2001. The inflammatory action of CD40 ligand (CD154) expressed on activated human platelets is temporally limited by coexpressed CD40. *Blood* 98: 1047–1054.
7. Duffau, P., J. Seneschal, C. Nicco, C. Richez, E. Lazaro, I. Douchet, C. Bordes, J. F. Viallard, C. Goulvestre, J. L. Pellegrin, et al. 2010. Platelet CD154 potentiates interferon-alpha secretion by plasmacytoid dendritic cells in systemic lupus erythematosus. *Sci. Transl. Med.* 2: 47ra63.
8. Arduin, E., S. Arora, P. R. Bamert, T. Kuiper, S. Popp, S. Geisse, R. Grau, T. Calzascia, G. Zenke, and J. Kovarik. 2015. Highly reduced binding to high and low affinity mouse Fc gamma receptors by L234A/L235A and N297A Fc mutations engineered into mouse IgG2a. *Mol. Immunol.* 63: 456–463.
9. Baudino, L., Y. Shinohara, F. Nimmerjahn, J. Furukawa, M. Nakata, E. Martinez-Soria, F. Petry, J. V. Ravetch, S. Nishimura, and S. Izui. 2008. Crucial role of aspartic acid at position 265 in the CH2 domain for murine IgG2a and IgG2b Fc-associated effector functions. *J. Immunol.* 181: 6664–6669.
10. Lund, J., N. Takahashi, J. D. Pound, M. Goodall, and R. Jefferis. 1996. Multiple interactions of IgG with its core oligosaccharide can modulate recognition by complement and human Fc gamma receptor I and influence the synthesis of its oligosaccharide chains. *J. Immunol.* 157: 4963–4969.
11. van Kooten, C., J. S. Gerritsma, M. E. Paape, L. A. van Es, J. Banchereau, and M. R. Daha. 1997. Possible role for CD40-CD40L in the regulation of interstitial infiltration in the kidney. *Kidney Int.* 51: 711–721.
12. Yellin, M. J., V. D'Agati, G. Parkinson, A. S. Han, A. Szema, D. Baum, D. Estes, M. Szabolcs, and L. Chess. 1997. Immunohistologic analysis of renal CD40 and CD40L expression in lupus nephritis and other glomerulonephritides. *Arthritis Rheum.* 40: 124–134.
13. Delmas, Y., J. F. Viallard, A. Solanilla, J. Villeneuve, J. M. Pasquet, F. Belloc, I. Dubus, J. Déchanet-Merville, P. Merville, P. Blanco, et al. 2005. Activation of mesangial cells by platelets in systemic lupus erythematosus via a CD154-dependent induction of CD40. *Kidney Int.* 68: 2068–2078.
14. Lambert, P. H., and F. J. Dixon. 1968. Pathogenesis of the glomerulonephritis of NZB/W mice. *J. Exp. Med.* 127: 507–522.
15. Theofilopoulos, A. N., and F. J. Dixon. 1985. Murine models of systemic lupus erythematosus. *Adv. Immunol.* 37: 269–390.
16. Lavoie, T. N., B. H. Lee, and C. Q. Nguyen. 2011. Current concepts: mouse models of Sjögren's syndrome. *J. Biomed. Biotechnol.* 2011: 549107.
17. Nusair, S., and A. Rubinow. 1999. The use of oral pilocarpine in xerostomia and Sjögren's syndrome. *Semin. Arthritis Rheum.* 28: 360–367.
18. Bagavant, H., M. Trzeciak, J. Papinska, I. Biswas, M. L. Dunkleberger, A. Sosnowska, and U. S. Deshmukh. 2018. A method for the measurement of salivary gland function in mice. *J. Vis. Exp.* (131): e57203.
19. Bethunaickan, R., C. C. Berthier, W. Zhang, R. Eksi, H. D. Li, Y. Guan, M. Kretzler, and A. Davidson. 2014. Identification of stage-specific genes associated with lupus nephritis and response to remission induction in (NZB × NZW)F1 and NZM2410 mice. *Arthritis Rheumatol.* 66: 2246–2258.
20. Rönnblom, L., and M. L. Eloranta. 2013. The interferon signature in autoimmune diseases. *Curr. Opin. Rheumatol.* 25: 248–253.
21. Baechler, E. C., F. M. Batliwalla, G. Karypis, P. M. Gaffney, W. A. Ortmann, K. J. Espe, K. B. Shark, W. J. Grande, K. M. Hughes, V. Kapur, et al. 2003. Interferon-inducible gene expression signature in peripheral blood cells of patients with severe lupus. *Proc. Natl. Acad. Sci. USA* 100: 2610–2615.
22. Bennett, L., A. K. Palucka, E. Arce, V. Cantrell, J. Borvak, J. Banchereau, and V. Pascual. 2003. Interferon and granulopoiesis signatures in systemic lupus erythematosus blood. *J. Exp. Med.* 197: 711–723.
23. Crow, M. K., K. A. Kirou, and J. Wohlgemuth. 2003. Microarray analysis of interferon-regulated genes in SLE. *Autoimmunity* 36: 481–490.
24. Han, G. M., S. L. Chen, N. Shen, S. Ye, C. D. Bao, and Y. Y. Gu. 2003. Analysis of gene expression profiles in human systemic lupus erythematosus using oligonucleotide microarray. *Genes Immun.* 4: 177–186.
25. Furie, R., M. Khamashta, J. T. Merrill, V. P. Werth, K. Kalunian, P. Brohawn, G. G. Illei, J. Drappa, L. Wang, and S. Yoo; CD1013 Study Investigators. 2017. Anifrolumab, an anti-interferon-α receptor monoclonal antibody, in moderate-to-severe systemic lupus erythematosus. *Arthritis Rheumatol.* 69: 376–386.
26. Khamashta, M., J. T. Merrill, V. P. Werth, R. Furie, K. Kalunian, G. G. Illei, J. Drappa, L. Wang, and W. Greth; CD1067 Study Investigators. 2016. Sifalimumab, an anti-interferon-α monoclonal antibody, in moderate to severe systemic lupus erythematosus: a randomised, double-blind, placebo-controlled study. *Ann. Rheum. Dis.* 75: 1909–1916.
27. Dimitriou, I. D., E. K. Kapsogeorgou, H. M. Moutsopoulos, and M. N. Manoussakis. 2002. CD40 on salivary gland epithelial cells: high constitutive expression by cultured cells from Sjögren's syndrome patients indicating their intrinsic activation. *Clin. Exp. Immunol.* 127: 386–392.
28. Park, J., R. Shrestha, C. Qiu, A. Kondo, S. Huang, M. Werth, M. Li, J. Barasch, and K. Suszták. 2018. Single-cell transcriptomics of the mouse kidney reveals potential cellular targets of kidney disease. *Science* 360: 758–763.
29. Tveita, A. A., Y. Ninomiya, Y. Sado, O. P. Rekvig, and S. N. Zykova. 2009. Development of lupus nephritis is associated with qualitative changes in the glomerular collagen IV matrix composition. *Lupus* 18: 355–360.
30. Verbinnen, B., A. D. Billiau, J. Vermeiren, G. Galicia, D. M. Bullens, L. Boon, P. Cadot, G. Hens, C. Dewolf-Peeters, S. W. Van Gool, and J. L. Ceuppens. 2008. Contribution of regulatory T cells and effector T cell deletion in tolerance induction by costimulation blockade. *J. Immunol.* 181: 1034–1042.
31. Vogel, I., B. Verbinnen, S. Van Gool, and J. L. Ceuppens. 2016. Regulatory T cell-dependent and -independent mechanisms of immune suppression by CD28/B7 and CD40/CD40L costimulation blockade. *J. Immunol.* 197: 533–540.
32. Mohan, C., Y. Shi, J. D. Laman, and S. K. Datta. 1995. Interaction between CD40 and its ligand gp39 in the development of murine lupus nephritis. *J. Immunol.* 154: 1470–1480.
33. Mahmoud, T. I., J. Wang, J. L. Karnell, Q. Wang, S. Wang, B. Naiman, P. Gross, P. Z. Brohawn, C. Morehouse, J. Aoyama, et al. 2016. Autoimmune manifestations in aged mice arise from early-life immune dysregulation. *Sci. Transl. Med.* 8: 361ra137.
34. Early, G. S., W. Zhao, and C. M. Burns. 1996. Anti-CD40 ligand antibody treatment prevents the development of lupus-like nephritis in a subset of New Zealand black x New Zealand white mice. Response correlates with the absence of an anti-antibody response. *J. Immunol.* 157: 3159–3164.
35. Kalled, S. L., A. H. Cutler, S. K. Datta, and D. W. Thomas. 1998. Anti-CD40 ligand antibody treatment of SNF1 mice with established nephritis: preservation of kidney function. *J. Immunol.* 160: 2158–2165.
36. Shock, A., L. Burkly, I. Wakefield, C. Peters, E. Garber, J. Ferrant, F. R. Taylor, L. Su, Y. M. Hsu, D. Hutto, et al. 2015. CDP7657, an anti-CD40L antibody lacking an Fc domain, inhibits CD40L-dependent immune responses without thrombotic complications: an in vivo study. *Arthritis Res. Ther.* 17: 234.
37. Kato, K., E. Santana-Sahagún, L. Z. Rassenti, M. H. Weisman, N. Tamura, S. Kobayashi, H. Hashimoto, and T. J. Kipps. 1999. The soluble CD40 ligand sCD154 in systemic lupus erythematosus. *J. Clin. Invest.* 104: 947–955.
38. Vakkalanka, R. K., C. Woo, K. A. Kirou, M. Koshy, D. Berger, and M. K. Crow. 1999. Elevated levels and functional capacity of soluble CD40 ligand in systemic lupus erythematosus sera. *Arthritis Rheum.* 42: 871–881.
39. Frese-Schaper, M., J. Zbaeren, M. Gugger, M. Monestier, and S. Frese. 2010. Reversal of established lupus nephritis and prolonged survival of New Zealand black x New Zealand white mice treated with the topoisomerase I inhibitor irinotecan. *J. Immunol.* 184: 2175–2182.
40. Rodriguez, W., C. Mold, M. Kataranovski, J. Hutt, L. L. Marnell, and T. W. Du Clos. 2005. Reversal of ongoing proteinuria in autoimmune mice by treatment with C-reactive protein. *Arthritis Rheum.* 52: 642–650.
41. Lin, W., D. Seshasayee, W. P. Lee, P. Caplazi, S. McVay, E. Suto, A. Nguyen, Z. Lin, Y. Sun, L. DeForge, et al. 2015. Dual B cell immunotherapy is superior to individual anti-CD20 depletion or BAFF blockade in murine models of spontaneous or accelerated lupus. *Arthritis Rheumatol.* 67: 215–224.
42. Bekar, K. W., T. Owen, R. Dunn, T. Ichikawa, W. Wang, R. Wang, J. Barnard, S. Brady, S. Nevarez, B. I. Goldman, et al. 2010. Prolonged effects of short-term anti-CD20 B cell depletion therapy in murine systemic lupus erythematosus. *Arthritis Rheum.* 62: 2443–2457.
43. Daikh, D. I., and D. Wofsy. 2001. Cutting edge: reversal of murine lupus nephritis with CTLA4Ig and cyclophosphamide. *J. Immunol.* 166: 2913–2916.
44. Ramanujam, M., X. Wang, W. Huang, L. Schiffer, C. Grimaldi, A. Akkerman, B. Diamond, M. P. Madaio, and A. Davidson. 2004. Mechanism of action of transmembrane activator and calcium modulator ligand interactor-Ig in murine systemic lupus erythematosus. *J. Immunol.* 173: 3524–3534.
45. Baccala, R., R. Gonzalez-Quintial, R. D. Schreiber, B. R. Lawson, D. H. Kono, and A. N. Theofilopoulos. 2012. Anti-IFN-alpha/beta receptor antibody treatment ameliorates disease in lupus-predisposed mice. *J. Immunol.* 189: 5976–5984.
46. Lesley, R., L. M. Kelly, Y. Xu, and J. G. Cyster. 2006. Naive CD4 T cells constitutively express CD40L and augment autoreactive B cell survival. *Proc. Natl. Acad. Sci. USA* 103: 10717–10722.
47. Miga, A. J., S. R. Masters, B. G. Durell, M. Gonzalez, M. K. Jenkins, C. Maliszewski, H. Kikutani, W. F. Wade, and R. J. Noelle. 2001. Dendritic cell longevity and T cell persistence is controlled by CD154-CD40 interactions. *Eur. J. Immunol.* 31: 959–965.
48. Haraldsson, B., J. Nyström, and W. M. Deen. 2008. Properties of the glomerular barrier and mechanisms of proteinuria. *Physiol. Rev.* 88: 451–487.
49. Jalanko, H., J. Patrakka, K. Tryggvason, and C. Holmberg. 2001. Genetic kidney diseases disclose the pathogenesis of proteinuria. *Ann. Med.* 33: 526–533.

50. Rigothier, C., R. Daculsi, S. Lepreux, P. Auguste, J. Villeneuve, A. Dewitte, E. Doudnikoff, M. Saleem, C. Bourget, C. Combe, and J. Ripoche. 2016. CD154 induces matrix metalloproteinase-9 secretion in human podocytes. *J. Cell. Biochem.* 117: 2737–2747.
51. Delville, M., T. K. Sigdel, C. Wei, J. Li, S. C. Hsieh, A. Fornoni, G. W. Burke, P. Bruneval, M. Naesens, A. Jackson, et al. 2014. A circulating antibody panel for pretransplant prediction of FSGS recurrence after kidney transplantation. *Sci. Transl. Med.* 6: 256ra136.
52. Ruth, A. J., A. R. Kitching, T. J. Semple, P. G. Tipping, and S. R. Holdsworth. 2003. Intrinsic renal cell expression of CD40 directs Th1 effectors inducing experimental crescentic glomerulonephritis. *J. Am. Soc. Nephrol.* 14: 2813–2822.
53. Foy, T. M., J. D. Laman, J. A. Ledbetter, A. Aruffo, E. Claassen, and R. J. Noelle. 1994. gp39-CD40 interactions are essential for germinal center formation and the development of B cell memory. *J. Exp. Med.* 180: 157–163.
54. Foy, T. M., D. M. Shepherd, F. H. Durie, A. Aruffo, J. A. Ledbetter, and R. J. Noelle. 1993. In vivo CD40-gp39 interactions are essential for thymus-dependent humoral immunity. II. Prolonged suppression of the humoral immune response by an antibody to the ligand for CD40, gp39. *J. Exp. Med.* 178: 1567–1575.
55. Crotty, S. 2011. Follicular helper CD4 T cells (TFH). *Annu. Rev. Immunol.* 29: 621–663.
56. Kyttaris, V. C., Z. Zhang, V. K. Kuchroo, M. Oukka, and G. C. Tsokos. 2010. Cutting edge: IL-23 receptor deficiency prevents the development of lupus nephritis in C57BL/6-lpr/lpr mice. *J. Immunol.* 184: 4605–4609.
57. Takahashi, S., L. Fossati, M. Iwamoto, R. Merino, R. Motta, T. Kobayakawa, and S. Izui. 1996. Imbalance towards Th1 predominance is associated with acceleration of lupus-like autoimmune syndrome in MRL mice. *J. Clin. Invest.* 97: 1597–1604.
58. Paust, H. J., J. E. Turner, O. M. Steinmetz, A. Peters, F. Heymann, C. Hölscher, G. Wolf, C. Kurts, H. W. Mittrücker, R. A. Stahl, and U. Panzer. 2009. The IL-23/Th17 axis contributes to renal injury in experimental glomerulonephritis. *J. Am. Soc. Nephrol.* 20: 969–979.
59. Kitching, A. R., S. R. Holdsworth, and P. G. Tipping. 2000. Crescentic glomerulonephritis--a manifestation of a nephritogenic Th1 response? *Histol. Histopathol.* 15: 993–1003.
60. de la Morena, M. T. 2016. Clinical phenotypes of hyper-IgM syndromes. *J. Allergy Clin. Immunol. Pract.* 4: 1023–1036.
61. van Vollenhoven, R. F., R. M. Fleischmann, D. E. Furst, S. Lacey, and P. B. Lehane. 2015. Longterm safety of rituximab: final report of the rheumatoid arthritis global clinical trial program over 11 Years. *J. Rheumatol.* 42: 1761–1766.
62. Gladman, D. D., F. Hussain, D. Ibañez, and M. B. Urowitz. 2002. The nature and outcome of infection in systemic lupus erythematosus. *Lupus* 11: 234–239.
63. Chamberlain, C., P. J. Colman, A. M. Ranger, L. C. Burkly, G. I. Johnston, C. Otoul, C. Stach, M. Zamacona, T. Dörner, M. Urowitz, and F. Hiepe. 2017. Repeated administration of dapirolizumab pegol in a randomised phase I study is well tolerated and accompanied by improvements in several composite measures of systemic lupus erythematosus disease activity and changes in whole blood transcriptomic profiles. [Published erratum appears in 2018 *Ann. Rheum. Dis.* 77: 787–788.] *Ann. Rheum. Dis.* 76: 1837–1844.